Scanning Microscopy

Volume 7 | Number 3 Article 1

8-2-1993

New Methods for Depositing and Imaging Molecules in Scanning Tunneling Microscopy

Victor N. Morozov
New York University

Nadrian C. Seeman
New York University

Neville R. Kallenbach
New York University

Scanning Microscopy, Vol. 7, No. 3, 1993 (Pages 757-779) 0891-7035/93$5.00+.00
Scanning Microscopy International, Chicago (AMF O'Hare), IL 60666 USA

NEW METHODS FOR DEPOSITING AND IMAGING MOLECULES IN SCANNING TUNNELING MICROSCOPY

Victor N. Morozov[1,*], Nadrian C. Seeman and Neville R. Kallenbach

W.M. Keck Foundation Laboratories for Biomolecular Imaging,
Department of Chemistry, New York University, New York, NY 10003, U.S.A.
[1]Permanent address: Institute of Theoretical and Experimental Biophysics of the Russian Academy of Sciences, Pushchino, Moscow Region, 142292 Russia.

(Received for publication November 17, 1992, and in revised form August 2, 1993)

Abstract

Methods and apparatus are described to deposit and image molecules by scanning tunneling microscopy (STM) under an inert atmosphere. Three methods of applying molecules have been evaluated: equilibrium adsorption from the vapor phase, sublimation, and electrospraying. Using these methods, a variety of organic and biopolymer molecules have been deposited and imaged on graphite and on gold (111), grown epitaxially on mica. Compared with alternatives, such as the use of high vacuum apparatus or glove boxes, these procedures offer some important advantages: they are inexpensive, convenient, and more rapid. Mercaptoethanol, ethanolamine, ethanol, acetic acid, and water produce two-dimensional crystalline adlayers on gold substrates, when they are introduced into the scanning cell as vapors. These adlayers are assumed to involve hydrogen bonding of the molecules to an oxide of gold formed on the surface. Electrospraying protein solutions on gold surfaces yielded images of individual protein molecules with lateral dimensions close to those measured by X-ray analysis, and thicknesses of 0.6-1.3 nm. In the case of metallothionein, the known internal domain structure of the molecule was reproducibly observed. No detailed internal structure could be resolved in the other examples examined.

Key Words: Scanning tunneling microscopy, Au(111), highly oriented pyrolytic graphite (HOPG), deposition methods, electrospray, sublimation.

*Address for correspondence:
Victor N. Morozov
W.M. Keck Foundation Laboratories
for Biomolecular Imaging,
Department of Chemistry,
New York University,
31 Washington Place, Room 1004, Box 116,
New York, NY 10003, U.S.A.
Telephone number: (212) 998 8465
FAX number: (212) 260 7905

Introduction

Among the most significant factors that affect the reliability of imaging molecules with scanning tunneling microscopy (STM) are: (**1**) obtaining a uniform distribution over an atomically smooth surface, (**2**) preventing lateral diffusion on storage, and (**3**) avoiding mechanical displacement on scanning (a review of these problems has been recently published by Nawaz *et al.*, 1992).

The simplest and most reliable method of deposition is from a vapor or via sublimation of a solid. Excellent images of copper-phthalocynanine molecules on copper (100) crystal face (Lippel *et al.*, 1989), naphthalene molecules on Pt(111) (Hallmark *et al.*, 1991), and benzene on rhodium (111) (Ohtani *et al.*, 1988) have been obtained after sublimation of these compounds in ultra-high vacuum (HV). This method has been used recently only in HV, to avoid surface contamination and decomposition of the sublimating compound in air. Here, we describe a simple method of depositing molecules via sublimation in an inert atmosphere, which solves these problems without the use of costly HV techniques.

Nevertheless, many molecules of interest cannot be sublimated or evaporated without decomposition. The most frequently used method for applying such molecules is evaporation of a droplet of solution on the substrate. This simple method works well with liquid crystals (Smith *et al.*, 1989; Rabe and Buchholz, 1991; Buchholz and Rabe, 1992), but it is not free from serious shortcomings: For example, a highly non-uniform distribution of molecules results when this technique is used to deposit single polymer molecules (Nawaz *et al.*, 1992). Moreover, contact with the solvent may change greatly the binding ability of the substrate. Electrochemical methods of application from solutions provide a reasonable alternative in terms of convenience and reliability, and the possibility of controlling the surface state (Lindsay *et al.*, 1992), but they require contact of the surface with solvent and buffer components, which can compete with deposited molecules for binding sites on the surface.

Here we describe a new method of depositing non-volatile molecules for STM observation that is free

from the drawbacks mentioned above. In this method molecules are deposited in a gas phase in the form of ions obtained by the electrospray ionization process. Methods of electrospray (ES) ionization of molecules have been developed for mass-spectrometry (Meng *et al.*, 1988; Fenn *et al.*, 1989; Smith *et al.*, 1990; Alexandrov *et al.*, 1991; Ikonomu *et al.*, 1991; Krasnov *et al.*, 1991; McLuckey *et al.*, 1991; Chait and Kent, 1992). Not only large organic molecules and synthetic polymers, but biopolymers [proteins with molecular weight (mol. wt.) of up to 100 kD and oligonucleotides] have been shown to be ionized effectively in air or in a nitrogen atmosphere and then separated in the mass-spectrometer. The physical mechanism of ES ionization remains an object of intensive study. It is believed to be basically connected with the decay of dispersed charged liquid droplets when they reach the Rayleigh limit of stability on evaporation, and with a subsequent field evaporation of molecular ions from small (10-20 nm diameter) droplets in their extremely large electrostatic field (Alexandrov *et al.*, 1991; Ikonomu *et al.*, 1991). Polymer molecules are detected in the mass-spectrometer (MS) as multicharged ions (up to 60 charges per protein molecule), with a number of charges that is nearly proportional to their molecular weight (Fenn *et al.*, 1989). This could be interpreted as evidence for the complete unfolding of protein molecules in ES ionization, with a rod-like stretched conformation of charges uniformly distributed over the polypeptide chain. However, the observation of protein-ligand non-covalent complexes in mass-spectra (Ganem *et al.*, 1991) as well as the strong dependence of protein ionization upon the pH of the solution (Smith *et al.*, 1990; Chowdhury and Chait, 1991) show that the loss of secondary and tertiary structures does not necessarily accompany the ionization process in ES. Quite recently, ES method has been used to deposit DNA molecules (Thundat *et al.*, 1992).

We describe here some simple accessories for deposition of molecules and imaging them under an inert atmosphere, using a conventional commercial Nanoscope II instrument. This provides conditions for using substrates that are rapidly contaminated in ambient air. It is well known, for example, that even gold surfaces (not to mention those of more reactive metals) become rapidly contaminated on exposure to air (Smith, 1980; Roberts *et al.*, 1989, 1991). As compared to HV techniques, the ability to deposit and scan under a controlled atmosphere has the advantage of being less expensive and more convenient for both sample preparation and tip replacement. Simple estimates (see Appendix I) show that the surface contamination rate in ultra-pure inert gas (with impurity content less than 1-2 ppm) is roughly equivalent to a vacuum of 10^{-7}-10^{-10} Torr at room temperature. Recently, a controlled environment STM has been described by Roberts *et al.* (1991). In contrast to our flow cell, in which only the tip and sample are under argon, their design places the entire scanning unit in a gas-filled chamber, and it cannot be used with commercially available STM heads.

Materials and Methods

Materials

Gold (99.99%) and silver (99.999%) used to prepare substrates were purchased from Aldrich. Argon (ultrapure grade) and hydrogen were obtained from Matheson. Oxygen (extra-dry) was from the Linde Specialty Gases division of Union Carbide. Glycerol, 2-mercaptoethanol, 2-aminoethanol (99.3%), dithiothreitol, uridine, adenine, and cytidine were purchased from Sigma. Acetic acid was from Fisher Scientific, reagent grade. Decacyclene, coronene (99%), 2,3-naphthalocyanine (95%), copper-phthalocyanine (97%), Ni-phthalocyanine tetrasulfonic acid (tetrasodium salt), rubrene, 1,2;3,4-dibenzanthracene (97%), diethylene triamine (99%), and 1,2,4-triazole (98%) were obtained from Aldrich and used without further purification. Polyethylene glycols, with average mol. wts. of 1450, 2000, 4000, and 8000, were obtained from Sigma.

Sperm whale myoglobin (Mb), horse hemoglobin (Hb), and cytochrome-c (Cyt-c) were obtained from Sigma. $tRNA^{phe}$ was purchased from Boehringer Mannheim. Proteins and tRNA were extensively dialyzed against double-distilled water. Rabbit hepatic metallothionein (isoform I of metC, prepared as described by Kimura *et al.*, 1979, free and in complex with Zn ions) was the kind gift of Dr. James Canary.

Instrumentation. All images were acquired with a Digital Instruments Nanoscope II STM (Santa Barbara) equipped with a 450x450 nm scanning head. Most large scale images were recorded under conditions of constant current ("height" mode of the Nanoscope). Small atomically resolved images were recorded under constant height conditions ("current" mode of the Nanoscope). Bias voltage and tunneling current (i) were specially selected in each case. Their values are presented in the legends to images. Large scale images were usually taken with low scanning rates (2.6-4.3 Hz). Scanning rates for images at atomic resolution varied form 78 to 16 Hz.

The tips used were mostly commercially-available Pt/Ir Nanotips (Digital Instruments, Santa Barbara). Some of the images were obtained with tips prepared from a tungsten wire by the electrochemical etching procedure described by Fotino (1992). These show excellent performance when freshly prepared and stored under argon.

Support preparation. Gold and silver substrates with a predominant (111) texture were prepared by epitaxial growth of 120-200 nm thick metal film onto freshly cleaved mica sheets (Reichelt and Lutz, 1971; DeRose *et al.*, 1991). The mica substrate was heated before evaporation of the metals for 3-6 hours at 450-500°C in a vacuum of $3x10^{-7}$-$1x10^{-6}$ Torr. Gold and silver were evaporated using the electron gun of a Balzers model BAE-080-T evaporator for metal coating. The metal was placed in a wire basket 3 mm in diameter and 4 mm long, which had been twisted from tungsten or molybdenum wire (99.9%, Aldrich). A table-heater for the mica

was constructed from stainless steel polished plates with a nichrome wire heater insulated by mica sheets. Its temperature was controlled with a constantine-copper thermocouple, calibrated by the melting point (m.p.) of Al and Zn, and the boiling point (b.p.) of glycerol and water. The distance between the table and evaporation source was 4 cm. During the evaporation, the temperature of the heating table did not rise by more than 20°C.

Prior to evaporation, metal and basket were outgassed for 1 minute at a temperature slightly below the evaporation temperature. The rate of evaporation was controlled by a quartz monitor and was less than 0.2 nm/sec. Pressure during evaporation did not exceed $2x10^{-6}$ Torr. Some metal film preparations were annealed at 500°C and at $2\text{-}5x10^{-7}$ Torr for 1 hour.

After cooling, the vacuum chamber was filled with argon and metal-covered mica was placed in a Pyrex tube using long pincers. The Pyrex tube had been outgassed in the HV chamber during the entire evaporation procedure. The mica sheet was then cut inside the argon-filled tube into 2 mm x 4 mm size samples.

Gold samples stored for more than 10 hours usually required preheating before deposition. This was done in an air- or oxygen-filled quartz oven at a temperature of 500°C for 3-15 minutes. After such baking, the sample was dropped into an argon-filled tube and transported to the scanning cell. At each stage, contact with air was minimized.

Flow-through scanning cell. The design of the scanning cell enables deposition of molecules via ES and their imaging under a controlled atmosphere, as shown schematically in Figure 1. The cell wall is made of a quartz cylinder with polished edges. The cylinder is glued to a perforated stainless steel base. Argon penetrates the cell through a small number of radially drilled holes in the base plate. The base plate is made of two parts, connected by welding. A system of grooves is milled in the base to allow the distribution of gas and the insertion of two sample-holding clamps made of tungsten wire. The cell is covered by a glass plate with a 1 mm diameter hole in the middle to allow the scanning needle to penetrate the cell. The covering plate is clamped with a double armed brass spring. This spring has two grooves, one on each side, to fix sample clamping springs. The design of the spring as well as its attachment to the double-walled base plate are illustrated in Figure 1.

To introduce vapor into the cell, a thin plastic tube is fitted to the STM needle as shown in Figure 1. This allows one to change rapidly the gas inside the cell and to avoid strong contamination of the cell and of the main gas inlet, which is observed when the main gas inlet is used to introduce the vapor.

The cell is glued to an STM-removable table with a cyanoacrylic glue. It is supplied with argon via a tube made from a number of 10 cm long stainless steel tubes (0.8 mm inside diameter, i.d.) connected by short plastic tubes. This arrangement was made to diminish contamination of argon with air components diffused through the

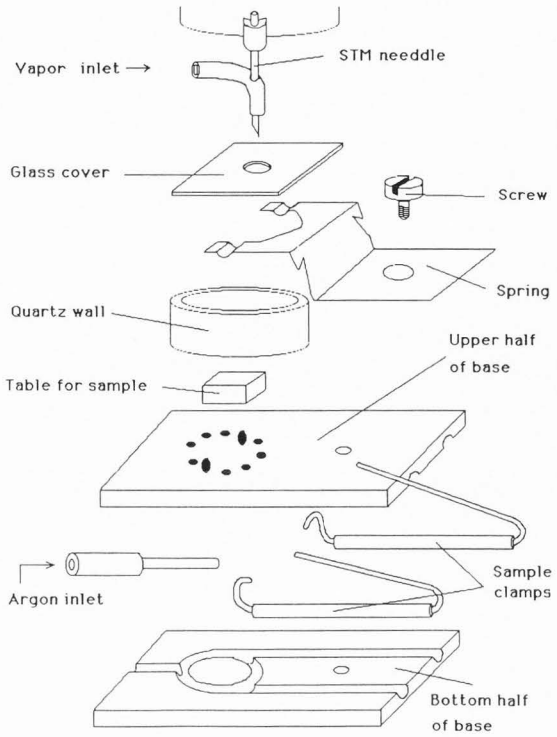

Figure 1. An exploded view of a flow-through chamber for taking STM images under inert atmosphere.

plastic wall on the way to the cell. Stainless steel tubes were outgassed before use by heating them to 700-800°C in argon.

Deposition methods

Direct application. A small droplet (10-20 μl) of solution was applied to the surface of the sample within the scanning cell and allowed to evaporate slowly in a weak flow of argon.

Equilibrium adsorption from vapor. This method was used to apply small molecules, usually liquids with a low boiling temperature. Argon was saturated by slow bubbling through the liquid, and then was introduced into the scanning cell via the plastic tube fitted on the scanning needle of the STM, as shown in Figure 1. The flow of argon (0.3 ml/sec) was maintained constant by means of a peristaltic pump. During deposition, the flow of argon into the cell through the main inlet was considerably reduced.

Sublimation. In this method, both substrate and a dry crystalline powdered compound were placed 1-2 cm apart, in a horizontally positioned glass tube of 5 mm inner diameter. A flow of argon (1-3 ml/sec) was put through the tube in the direction from the powdered substance to the substrate. The tube was then heated locally under the powdered substance with an electric heater, until visible condensation of vapor appeared on cold walls of the tube. In some cases, the substrate was also heated to promote two-dimensional crystallization.

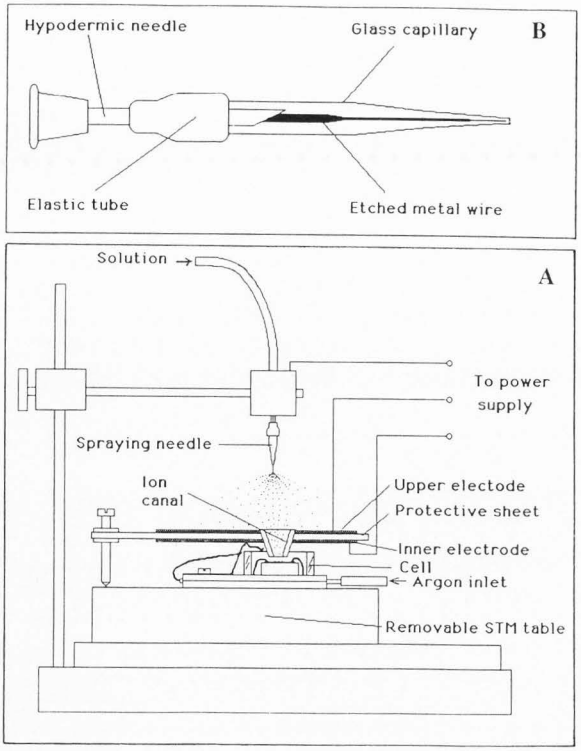

Figure 2. Schematic representation of accessories for the electrospray deposition of molecules onto surfaces protected from contact with air. **A.** Schematic of the deposition process. **B.** Design of the electrospray needle.

Electrospray method. Easy-to-make accessories (shown schematically in Figures 2A and 2B) were designed for this purpose. A spraying needle was made from a hypodermic stainless steel needle with a glass capillary attached. They were connected with an elastic plastic tube as shown in Figure 2B. A tungsten wire electrochemically etched to about 10-20 μm in diameter made electrical contact between the hypodermic needle and the tip of the glass capillary. As compared with previously described designs for spraying needles (Meng *et al.*, 1988; Smith *et al.*, 1990; Chowdhury and Chait, 1991; Ikonomu *et al*, 1991) the present arrangement is advantageous for spraying aqueous solutions, since the tip size can be easily made as small as 20-50 μm in diameter. A small tip diameter is known to facilitate spraying of liquids with high surface tension, before the corona discharge limit is reached (Chowdhury and Chait, 1991).

In this variant of the ES device, we did not use a pump to maintain a constant rate of liquid supply. Instead, a low positive or negative pressure was applied to the liquid in the capillary, to obtain a fine spray cone (torch), in which microdroplets were not visible under a low-power microscope. The voltage applied to the capillary did not exceed 4000 V.

To enable deposition of ions on a sample placed within the scanning cell, where it is protected from contact with air, we used a protective sheet containing an ion canal, shown schematically in Figure 2A. After adjustment of spraying parameters (voltage and pressure) a 2-3 kV voltage was applied between the upper electrode of the protective sheet and the STM cell connected to the inner electrode. This electric field was directed to pump ions in, and to transport them through the plastic tube to the substrate surface. The spraying uniformity was checked using a slightly wetted piece of paper as a sample. It was found that about 1-5% of all sprayed molecules reach the substrate surface. The deposition density has a broad maximum under the central part of the canal and smoothly decreases to its periphery. In the absence of voltage applied to the protective sheet or voltage of the opposite sign, no dye deposition was observed on the paper, even after spraying a large volume of dye solution. This control experiment permits one to roughly estimate the volume of solution that needs to be electrosprayed in order to have the required deposition density. For example, after spraying 1 μl of a 1 μM solution, we have more than $0.01 \times 6 \times 10^{11}$ ($= 6 \times 10^{9}$) molecules per 10 mm^2 of substrate, which provides an average deposition density of more than 600 molecules/μm^2. Whereas, these molecules are not randomly distributed, we may choose a deposition density convenient for scanning by shifting the position of the scanning needle in a radial fashion.

The concentrations of protein solutions used for ES deposition were 0.1-1 mg/ml. Larger concentrations have been shown to lower the efficiency of ES (Ikonomu *et al.*, 1991). Good ES was obtained for aqueous solutions only with a positive potential at the needle. Water-organic mixtures were readily sprayed at both positive and negative potentials.

Scanning procedures for imaging adsorbate molecules included: cleaning the prepared surface; control checking with 1-3 images; and applying the sample molecules and collecting images beginning with large bias voltages (2-3 V) and low tunneling current (0.2-0.4 nA). The bias voltage is subsequently decreased and the tunneling current increased until adsorbed molecules are seen to be pushed away by the tip. To observe direct binding of molecules from a vapor, optimal scanning parameters were first found by trial and error, and then adjusted before admitting vapor into the scanning cell. After introducing vapor into the cell, images of the same surface were recorded at regular intervals.

When observing crystalline adsorbates, images were routinely taken at different scanning rates (twice and half of the optimal rate) and with slight variations of the bias voltage ($\pm$50%) and tunneling current (+100%, -50%), to check the independence of the crystalline lattice parameters from the scanning parameters. This procedure eliminates the possibility that artifacts of the feed-back control system of the microscope are mistaken for authentic images.

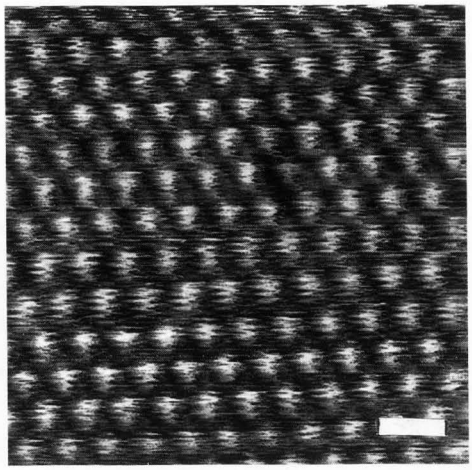

Figure 3. STM image of an epitaxially grown Au(111) surface. Bias voltage 24 mV, current 18 nA. Bar = 0.5 nm.

Results

Characterization of clean surfaces

Gold film on mica. Immediately after preparation, the atomic corrugation of the (111) face of gold crystal was visible. Occasionally, characteristic $22x\sqrt{3}$ reconstruction (Haiss *et al.*, 1991) was seen. An example of atomic gold corrugation is presented in Figure 3. However, this feature could be observed only in the first few hours after sample preparation. On further storage under argon, the surface became contaminated, with flakes of a few nm in size becoming visible at high bias voltage and low tunneling current. To enable use of the substrate in imaging of molecules under these conditions, the surface was briefly heated as described in **Methods**. Heat treatment removed the flakes from the surface, leaving a smooth surface ($\pm$ 0.5 nm), with no atomic crystalline structure resolved. After 7-10 days of storage under argon, the gold was found to be covered with a heavy adsorbate layer containing characteristic black holes a few nm in size, visible in the STM (Buchholz *et al.*, 1991). These surfaces did not resume a flat structure on heating, and were discarded.

Silver produced opaque films on mica. In the STM, very large flat crystalline planes were seen in every scan. However, we failed to observe the atomic corrugation of the Ag(111) plane on fresh films, or after heat treatment in air, oxygen or hydrogen. Ag films treated for 5-10 minutes at 500°C in hydrogen were free from flakes and contained readily visible large flat monatomic layers. They seemed to be suitable for imaging adsorbate molecules. As compared to gold layers, those of silver were considerably more fragile: Notable changes of their form could be observed even at large tip-to-surface gaps (current 0.2 nA, bias voltage 2500 mV). This instability of the silver surfaces discouraged us from using them as substrates for imaging adsorbed molecules.

Vapor deposition of samples

Of the nine volatile compounds tested in this procedure of deposition (2-mercaptoethanol, 2-aminoethanol, ethanol, acetic acid, water, 30% solution of ammonia, diethylenetriamine, dithiothreitol, n-butanol), only the first five showed a marked tendency to condense on gold surfaces, forming 2-dimensional crystalline lattices when introduced as vapor in the STM cell. Usually crystals appeared immediately after vapor penetrated the cell. First, one-dimensional linear arrays of spots appeared, running on the surface in the case of 2-mercaptoethanol and acetic acid. These arrays then coalesced to form polycrystalline 2-dimensional lattices. Substances which do not form crystalline layers, such as butanol or diethylenetriamine, nevertheless manifest their presence on the gold surface, by producing unstable smeared strips.

2-mercaptoethanol. Some variability of the lattices formed by these molecules was observed. The lattices observed predominantly with 2-mercaptoethanol are presented in Figures 4A and 4B. They have similar lattice parameters, $\mathbf{a} = 1.2 \pm 0.1$ nm; $\mathbf{b} = 1.0 \pm 0.1$ nm, $\gamma = 113 \pm 5°$, but the internal distribution of tunneling current is different within the images, taken under nearly identical scanning conditions. No systematic study of the dependence of images upon scanning has been performed. There is no doubt, however, that image structure depends upon scanning conditions and sample history. Thus, even at high bias (893 mV, i = 1.9 nA), 2-dimensional crystals similar to those presented in Figures 4A and 4B, appear immediately after admitting 2-mercaptoethanol vapor. A layered structure (we refer to it as 'lamellar'), with a distance between layers of about 1.6 nm, as seen in Figure 4C, appears later as a result of saturating the first layer or its reorganization (in upper left corner of Figure 4C, 2-dimensional crystals are seen together with lamellar structures). Decrease of current to 0.2 nA makes some white flakes, 2-4 nm in size, visible. Slow decrease in bias voltage resulted in removal of both the flakes and lamellar structures on reaching 65 mV (i = 1.9 nA), with only the 2-dimensional crystals remaining. A characteristic feature of gold surfaces covered with 2-mercaptoethanol is the emergence of black holes, which are clearly seen in Figures 4A and 4D. They appear immediately after adlayer formation, and occupy places between adlayer crystallites. These black holes seem to move by tip action.

Acetic acid produced structures markedly different from those observed in the presence of 2-mercaptoethanol. First, regular chains appeared with a periodicity of 0.3-0.4 nm (Fig. 5A), then, in about 15 minutes, a 2-dimensional superlattice of $\mathbf{a} = \mathbf{b} = 1.2$ nm, $\gamma = 100°$ forms with a visibly structured underlayer (Fig. 5B). Black holes occurred in this superlattice, but they were different from those seen with 2-mercaptoethanol. The adlayer of acetic acid appeared less densely packed, while the black holes were less regular and had different sizes (compare Figs. 5C and 4D).

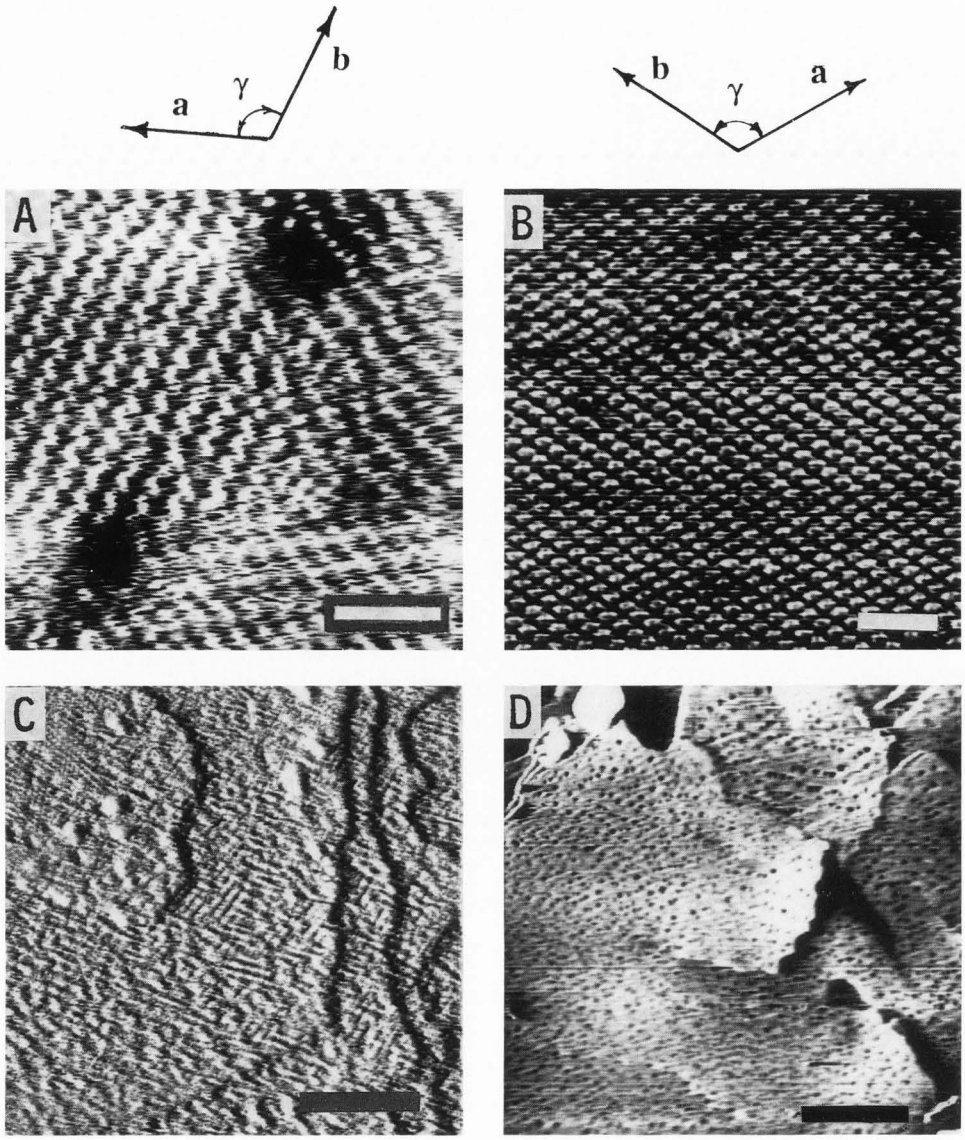

Figure 4. STM images of the (111) gold surface in the presence of 2-mercaptoethanol vapor in the cell. **A** and **B** are variants of the structures observed under different scanning conditions (**A**: tip bias -30 mV, current 1.8 nA; **B**: bias voltage -22 mV, current 3.1 nA). **C**. Lamellae structures observed at high bias voltage, 737 mV, current 1.6 nA. **D**. Large-scale image of the gold surface after deposition of 2-mercaptoethanol. Arrows at the top of A and B indicate choice of axes in the 2-dimensional crystal in the upper-left part of A and in B, respectively. Bars = 5 nm (A and B); 20 nm (C); and 100 nm (D).

2-aminoethanol produced a 2-dimensional lattice with unit cell parameters: **a** = 1.7 ± 0.05 nm, **b** = 1.5 ± 0.05 nm and γ = 106° (Fig. 6A). As in the previous cases, this seems to be a superlattice, based on a hexagonal layer with a lattice parameter of 0.48 ± 0.05 nm (Fig. 6B).

Ethanol produced rather polymorphic and unsteady 2-dimensional patterns. Their characteristic features were a lack of stability: They appeared, disappeared, and were displaced from scan to scan. In Figure 7A, the lattice parameters differed even within a single image. They varied from 3.9 nm to 5.5 nm in one direction, and had a more conservative size, 1.3 nm, in another. The generation of an ethanol lattice was clearly seen in the image. The crystals appeared as long broken strips, somewhat like those formed by running water droplets on a car windshield in the rain.

Water crystals (see Fig. 7B), though more stable, as compared to those of ethanol, also had highly variable lattice parameters, with changes from 0.8 to 2.1 nm in

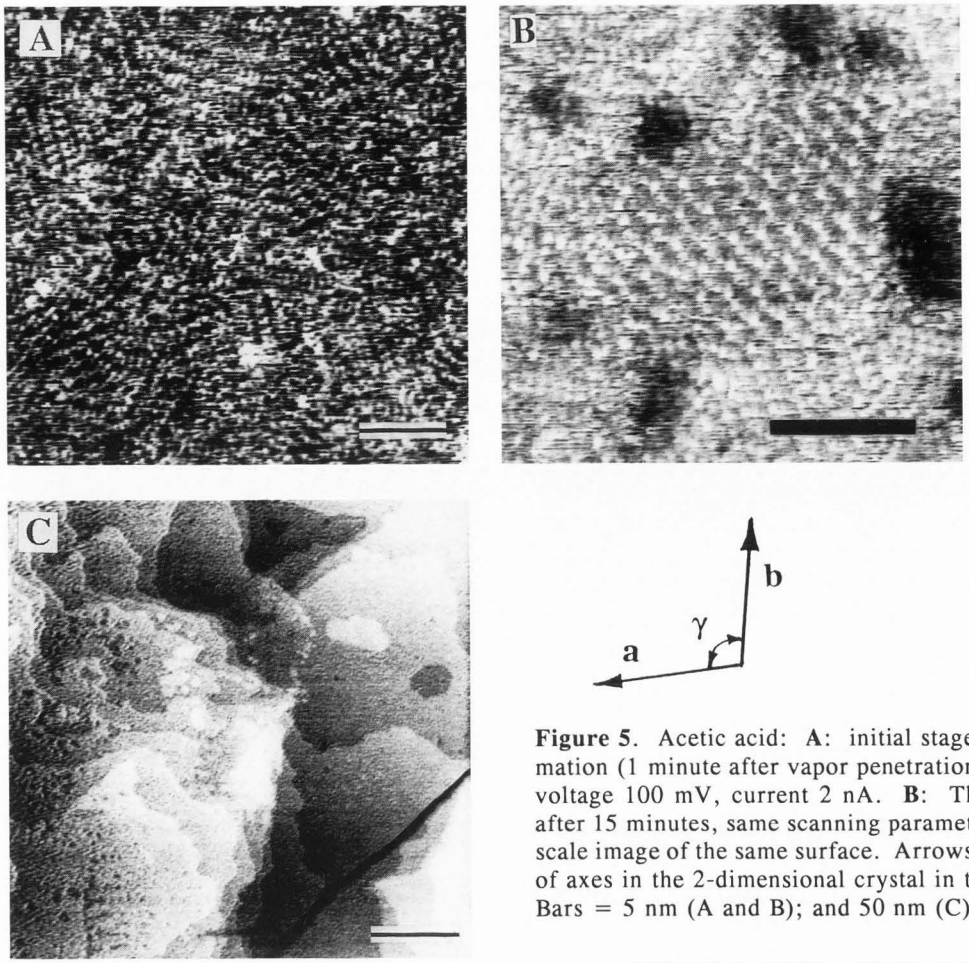

Figure 5. Acetic acid: **A**: initial stage of adlayer formation (1 minute after vapor penetration into cell), bias voltage 100 mV, current 2 nA. **B**: The same surface after 15 minutes, same scanning parameters. **C**: Large-scale image of the same surface. Arrows indicate choice of axes in the 2-dimensional crystal in the middle of B. Bars = 5 nm (A and B); and 50 nm (C).

dimension and in the unit cell shape (square and parallelogram lattices were seen in the images). Similar crystalline images were observed under different bias voltages (± 20 mV), currents (0.2-2 nA), scanning rates (39-18 Hz), and with different tips.

All the structures are readily reversible, except those of 2-mercaptoethanol: They fade out in a few minutes under a flow of pure argon. After a brief exposure, even 2-mercaptoethanol is reversible. However, after exposure to 2-mercaptoethanol vapor for 1 hour, the characteristic crystalline species of 2-mercaptoethanol can be found on a gold surface, even after 4 hours storage in a flow of pure argon. This is seen, even though the entire surface is not covered by the crystals. Even traces of 2-mercaptoethanol, desorbed from inner walls of the scanning cell, were able to produce crystals when a gold sample was left overnight in the cell with no argon flow. Experiments with 2-mercaptoethanol did not require pure gold surfaces. This ligand shows a remarkable ability to displace contaminants.

Deposition by sublimation

Sublimation was used to apply large molecules that are volatile only at high temperatures. Both highly oriented pyrolytic graphite (HOPG) and (111) gold surfaces were used in these experiments. Of the 11 organic molecules sublimated onto the HOPG surface (coronene, rubrene, decacyclene, 1,2;3,4-dibenzanthracene, 2,3-naphthalocyanine, Cu-phthalocyanine, adenine, cytidine, uridine, imidazole, and 1,2,4-triazole) only coronene and uridine were found to form crystalline layers in the STM (despite the presence of an apparently crystalline deposit on the HOPG surface, visible under an optical microscope, in all cases). The images of coronene, presented in Figures 8A and 8B were repeatedly observed when scanned after sublimation. Both, under argon and under a droplet of glycerol, coronene adlayer was always imaged as a hexagonal lattice with the same parameter, **a** = 1.1 ± 0.05 nm, and with the same ring-like appearance of the unit cell.

Uridine produced an image of a notably different crystal with lattice parameters **a** = 1.2 nm, **b** = 1.25 nm and $\gamma = 96°$. The image of uridine crystals was unstable. The crystalline lattice, presented in Figure 9, could be observed for only 2-3 scans, even at high gap; then the crystalline image disappeared and amorphous material was then concentrated on the image boundaries. After zooming into this amorphous region, the same

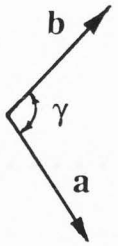

Figure 6. STM image of the Au(111) surface in contact with 2-aminoethanol vapor. **A** (at -22 mV and 2.9 nA) and **B** (at -259 mV and 2.9 nA) are variants of the structures observed at different scanning parameters. Arrows show choice of crystallographic directions for the lattice in the middle of A. Bars = 5 nm (A); and 1 nm (B).

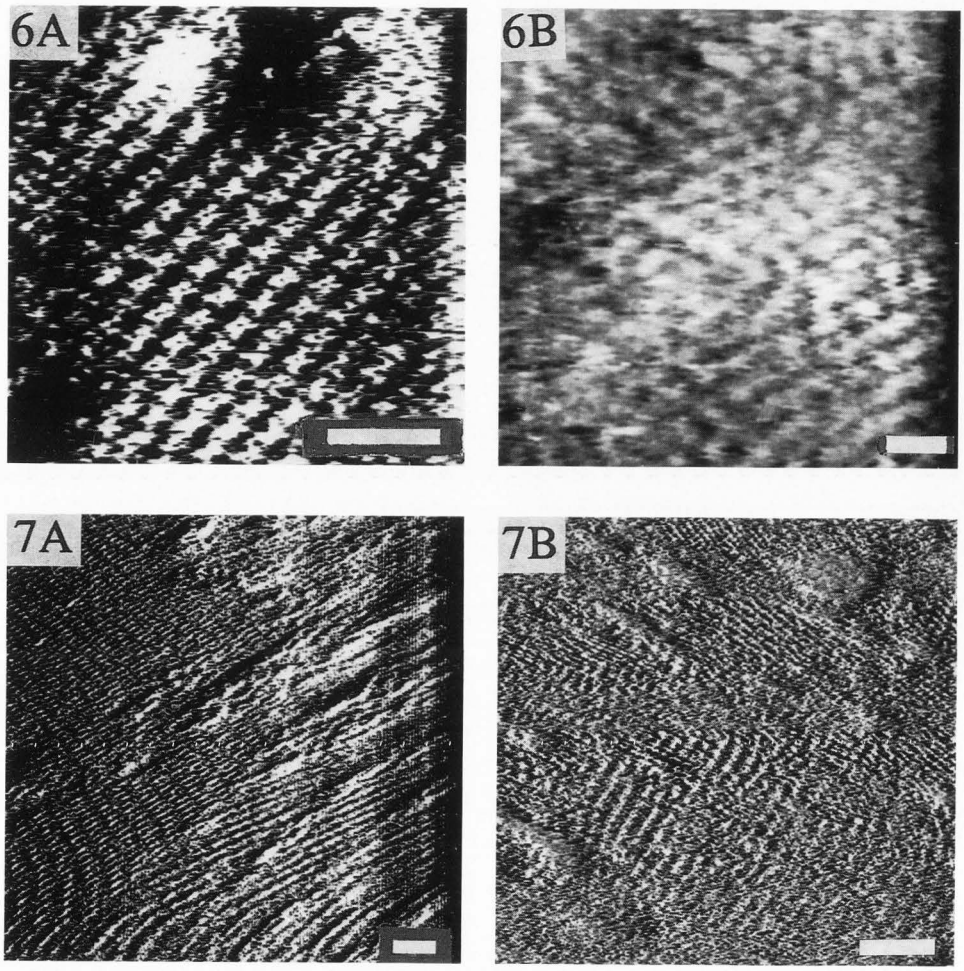

Figure 7. Polymorphic crystallinity on the Au(111) surface in contact with ethanol vapor (**A**) and water vapor (**B**). Scanning conditions: A: -247 mV and 2.4 nA; B: 22.9 mV and 2 nA. Bars = 10 nm.

Figure 8. STM image of coronene sublimated onto an HOPG surface. **A**: Scanning under argon, bias voltage is 17 mV, current is 1.1 nA. **B**: Scanning under glycerol, bias voltage is 780 mV, current is 0.54 nA. Bars = 5 nm.

Figure 9. STM image of uridine sublimated onto an HOPG basal plane. Bias voltage is 855 mV, current is 0.38 nA. Arrows indicate choice of crystallographic directions. Bar = 10 nm.

Figure 10. **A**. Image of copper-phthalocyanine molecules sublimated on the Au(111) surface. Tip bias 1320 mV, current 3,4 nA. **B**: zoom of the upper right part of the image presented in A. Bars = 5 nm (A); and 1 nm (B).

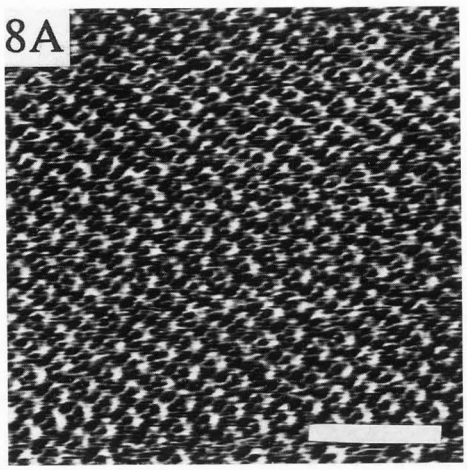

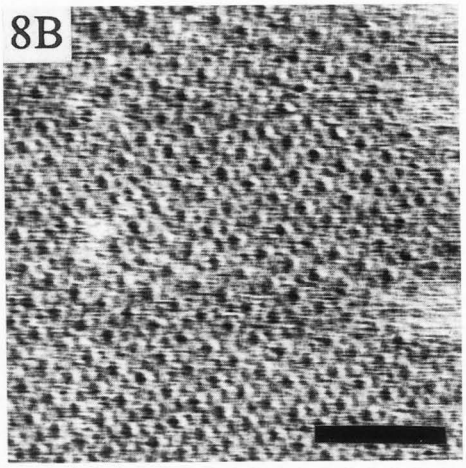

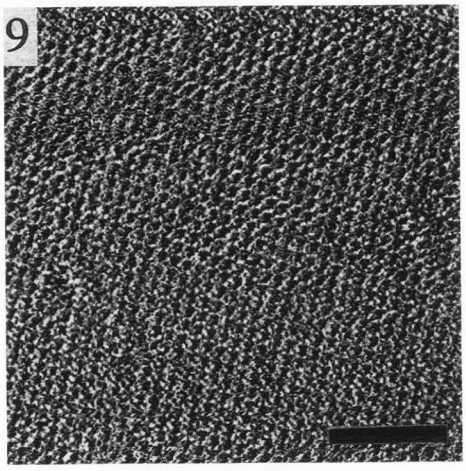

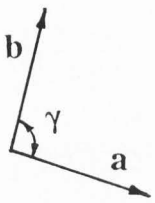

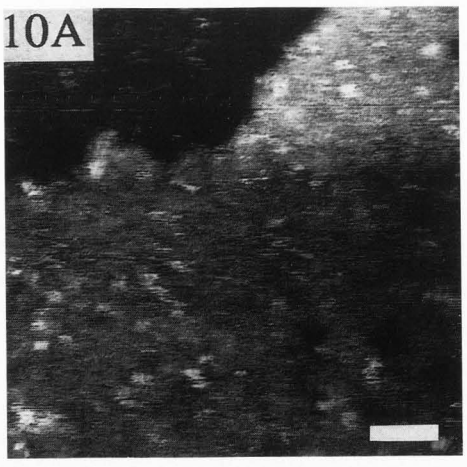

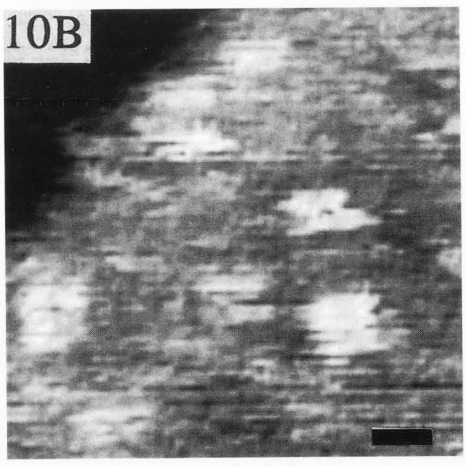

See captios for Figures 8-10 on the bottom of the facing page.

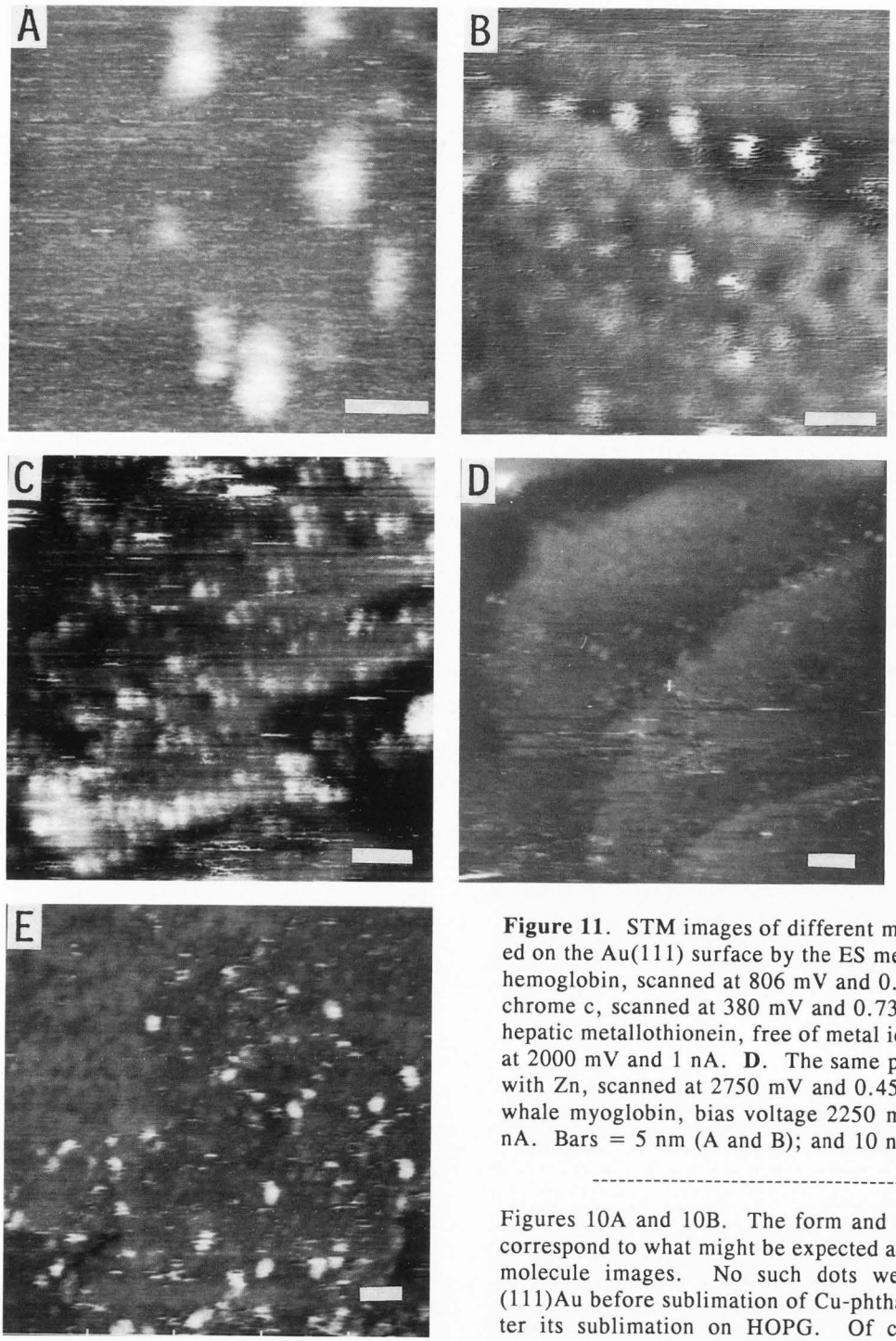

Figure 11. STM images of different molecules deposited on the Au(111) surface by the ES method. **A.** Horse hemoglobin, scanned at 806 mV and 0.5 nA. **B.** Cytochrome c, scanned at 380 mV and 0.73 nA. **C.** Rabbit hepatic metallothionein, free of metal ions, was scanned at 2000 mV and 1 nA. **D.** The same protein, saturated with Zn, scanned at 2750 mV and 0.45 nA. **E.** Sperm whale myoglobin, bias voltage 2250 mV, current 0.33 nA. Bars = 5 nm (A and B); and 10 nm (C, D and E).

---

crystalline lattice reappeared, only to disappear again after 2-3 scans. These crystals were detected in one of 3 samples tested.

Of two large molecules sublimated on the Au(111) substrate, coronene and Cu-phthalocyanine, only the latter was observed as single molecules, having the appearance of slightly distorted squares or crosses, as seen in Figures 10A and 10B. The form and size of the spots correspond to what might be expected as phthalocyanine molecule images. No such dots were observed on (111)Au before sublimation of Cu-phthalocyanine or after its sublimation on HOPG. Of course, it is not excluded, that dots corresponds to some impurity present in phthalocynaine sample.

Electrospray deposition

Proteins. ES deposition proved to be especially effective for proteins. With a number of monomeric proteins deposited on Au(111), we observed rather homogeneous-size spots of ellipsoidal form. A few examples of protein images are presented in Figures 11A to 11E. A

plot in Figure 12 shows that the correlation between sizes of monomeric proteins observed in our STM images and those known from X-ray analysis is quite satisfactory. What is very different from the X-ray size is the thickness of STM images: For proteins deposited from water solutions it varies from 1.2 to 1.3 nm for Mb and metallothionein, to 0.5 to 0.7 nm for other proteins studied. ES deposition of Mb from a mixture of 40% methanol, 40% acetonitrile, and 20% of water (routinely used in ES of proteins in mass-spectrometry) resulted in the same lateral sizes of images and a slight decrease in thickness (to 0.7-1 nm) in the latter case.

Control experiments with ES of pure water revealed no noticeable changes on the gold surface. Water electrosprayed at positive potential, used here, may penetrate the cell only in the form of stable hydronium ions, H_3O^+. On discharging on the gold surface, these produce water and hydrogen, which easily desorb from the surface (short exposures to water vapor and to pure hydrogen were shown to be completely and rapidly reversible). That explains why we did not see any changes of gold surface after electrospraying of water in control experiments.

Images of ES deposited hemoglobin were not as homogeneous in size as that of monomeric proteins. The fraction of monomer- and dimer-sized spots varied in different depositions of hemoglobin (see Figs. 11A and 13).

The image of each protein was observed only if the bias voltage exceeded a certain value, specific for each protein (45 mV at 0.6 nA for Hb, 380 mV at 0.73 nA for Cyt-c, and 1360 mV at 1 nA for metallothionein). On decreasing the bias voltage, protein molecules disappeared from the image one by one, and were then seen to form a frame; this frame was visible after raising the bias and zooming out to a larger image scale. The results of this experiment are shown in Figures 13A-13F for horse hemoglobin molecules. It should be noted that the stability of protein images was far more strongly dependent upon bias potential than on tunneling current. Whereas, a 20-30% decrease in the bias potential has, in some cases, pushed the molecules off the field, a tenfold increase in the tunneling current produced no noticeable effects.

In no case except metallothionein is internal structure of protein molecules recognizable in their STM images. Metallothionein molecules are shown in Figures 11C and 11D to have the appearance of double spots with slightly different sizes. This overall shape of the molecules is clearly seen in the X-ray crystal structure (Robins and Stout, 1991). Double spotted images prevailed in all cases when metallothionein is applied (two different samples of metC, with and without bound Zn ions), although single domains are present together with whole molecules in some samples (e.g, see, Fig. 11D). Observation of single domain images together with double-domain images in the same picture argues against a "double tip" artifact explanation of the metallothionein images (the first idea which comes to mind when looking

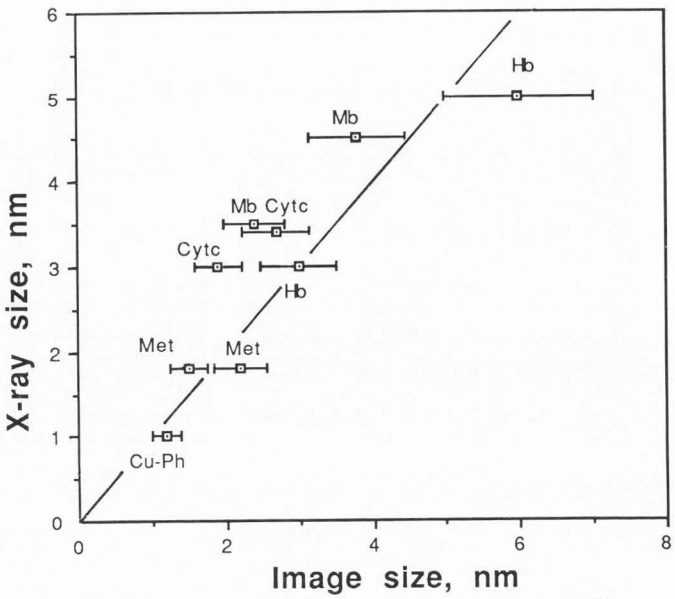

Figure 12. Plot of protein sizes obtained in STM images after ES deposition on a gold surface versus their X-ray sizes. X-ray sizes were taken from Stryer (1988). Of the three parameters of protein shape describing protein molecules as an ellipsoid, the two largest are taken to compare with the two elliptical parameters of the images. The size of the metallothionein domain was taken to be 0.18 nm (Robbins and Stout, 1991). Hemoglobin images were attributed to $\alpha\beta$-dimers. The line has a slope of 1.

---

at the images). It should be noted that metallothionein, when applied directly to the gold surface produces a heavy adsorbate layer with no globular structure visible at all.

Synthetic polymers, such as polyvinyl alcohol (PVC, of unidentified mol. wt.) and polyethylene glycols (PEG of average mol. wts. 1450, 2000, 4000, and 8000), deposited on gold by ES from water or ethanol solutions also were imaged as round or elongated objects, a few nm in size. An example of such an image is presented in Figure 14A for polyvinyl alcohol. In contrast to those of proteins, polymer images have a broader distribution of sizes. Polyethylene glycol molecules of high molecular weight are seen in Figure 14B to have the appearance of arrayed granular structures. The synthetic polymer images can be shifted easily to the edge of the screen by lowering the tip bias, similar to proteins. Although stable at 760 mV and 0.46 nA, PEG-4000 species could be removed by lowering the bias voltage to 430 mV at the same current, or by increasing the tunneling current to 2 nA at the same voltage. On reversal of the bias voltage, the images were considerably more stable, remaining in the field up to -20 mV at 1 nA.

We failed to obtain stable images of yeast t-RNA^{phe} deposited on gold. Formless spots, a few nm

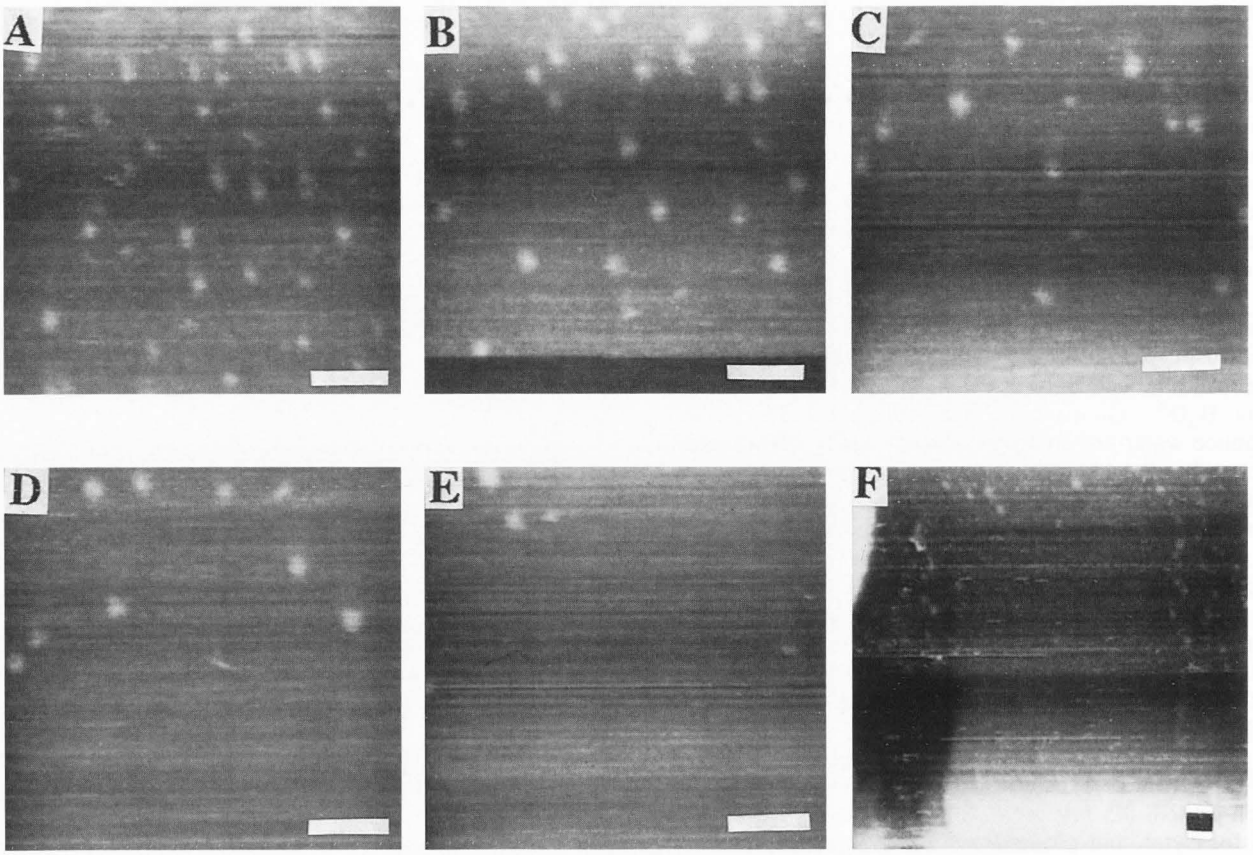

Figure 13. The effect of pushing protein molecules off the image field with decreasing tip-to-support gap. Each scan of hemoglobin molecules was taken at 0.6 nA with different tip bias voltages: 500 mV, 250 mV, 100 mV, 45 mV, and 22 mV for images **A**, **B**, **C**, **D**, and **E**, respectively. The image in **F** was taken after increasing the bias voltage to 1500 mV and zooming to 3 times larger scale. Bars = 10 nm.

in size, could be seen repeatedly; however, these spots changed in size and shape from scan to scan at high bias voltages (more than 2300 mV), and moved at slightly lower voltages.

Discussion

Flow-through scanning cell

As compared to the earlier technique of Roberts *et al.* (1991), or a glove box, the accessories described here have some important advantages:

(**a**) A plastic glove box is penetrable to air components. For example, 1.5×10^{-7} cm^3/sec of oxygen penetrates 1 square cm of polyethylene film (of 1 mm thickness) if it is in contact with air at room temperature (Sperling, 1992). Suppose, we have a cubic glove box of 1 liter volume made of 0.5 mm polyethylene, filled with ultrapure argon (say, having 1 ppm of oxygen). Then, it is easy to calculate, that within an hour, 0.64 ml of oxygen will penetrate the box increasing the impurity level 640 times!

(**b**) The small cell saves expensive noble gas, especially upon replacing air from the cell. The initial gas concentration, C, remaining in box with volume, V_o, after flowing a volume, V, of argon is described by a logarithmic function, $C(V) = C_o \exp(-V/V_o)$. Here C_o is the initial concentration of gas. To reduce concentration of air components in a 1 liter box to about 1 ppm, we need to pump 14 liters of argon, whereas a 0.3 ml cell requires only 4 ml.

(**c**) All the components of the STM head placed into a glove box will desorb impurities normally present on any metal or plastic surface. Simple estimates show that, even if made of steel (not to mention plastic that allows small molecules to dissolve in and penetrate

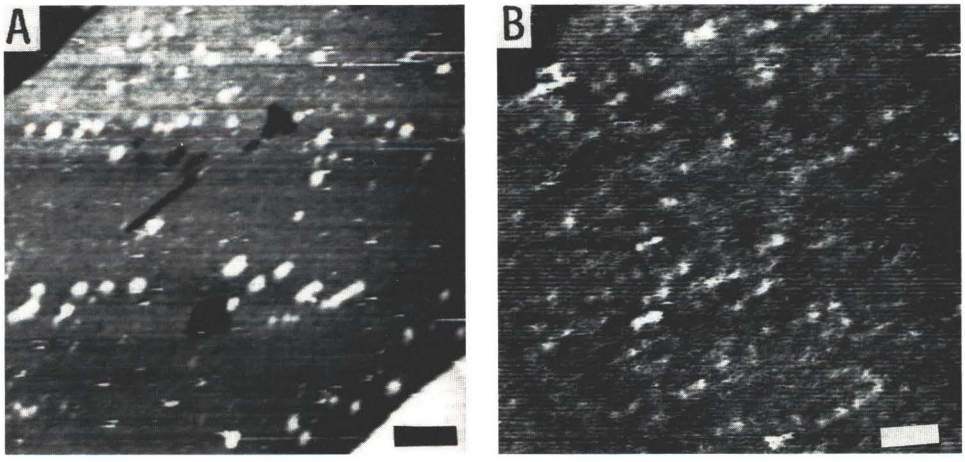

Figure 14. STM images of polyvinyl alcohol (**A**), and PEG (8000) (**B**), deposited by the ES method from an aqueous solutions on the Au(111) surface. Bias voltage is 847 mV, current is 0.28 nA in A; and 1610 mV and 0.19 nA in B. Bar = 20 nm (A); and 10 nm (B).

through), the box wells are capable of liberating $(1\text{-}7)\text{x}10^{19}$ molecules per m^2 of geometrical surface (Roth, 1976) and, thus, increasing the impurity concentration of argon in the above mentioned 1 liter box by a factor of 40-300.

(**d**) Placing the head in the atmosphere of active vapors, like mercaptans or halogens, risks corrosion or other undesirable side reactions. As an example, when iodine was used, a greatly increased leakage in the head occurred, and the apparatus could not be used for several hours.

Reliability

The major problem that has led to questions about the STM imaging of molecular adsorbates is that of the reliability of images. The data presented here, unless otherwise noted, can be observed repeatedly in every scan, following deposition of molecules. In vapor deposition, the same part of the surface is observed prior to deposition; with molecules adsorbed; and the same surface is then recorded following desorption of the adsorbate in a stream of pure argon. This procedure completely eliminates the possibility that occasional substrate features or contaminants can be mistaken for deposited molecules. In addition, the crystalline images were routinely taken at different scanning rates, and with slightly varied scanning parameters, to eliminate the possibility of artifacts due to the feed-back control system of the microscope. Typical of all the 2-dimensional lattices is their polycrystalline appearance, with different 2-dimensional monocrystals seen to be oriented differently, as it is clearly seen in Figures 4A, 5B and 7B. This excludes possible explanation of the images as artifacts resulting from some mechanical vibrations or oscillations in the feed-back control system of the STM. When the tip-surface gap is decreased, individual molecules are seen to be displaced to the sides of the image; this key characteristic distinguishes them from surface defects. Hence, there can be no doubt that the images presented here are not occasional surface defects, but result from the deposition of molecules. The combination of methods tested here allows nearly any type of molecule to be deposited and imaged under controlled conditions, provided a suitable surface is chosen as a substrate, i.e., smooth enough, and capable of anchoring single molecules or 2-dimensional arrays of them.

Substrates

The use of metal crystalline faces as substrates in STM studies is advantageous, since they provide strong and localized binding of deposited species. Of all the metals, gold seems to be most convenient both in preparation (it readily forms relatively large flat atomic terraces) and in handling, since contamination of the gold surface proceeds less rapidly than that of other (non-noble) metals. Nevertheless, it needs to be protected from contact with the atmosphere when used in STM studies. The simple accessories described here seem to provide effective protection of the gold surface, for both deposition and scanning procedures.

The preparation of crystalline films from other noble metals, such as platinum, poses technical difficulties, requiring considerably higher evaporation and annealing temperatures (873-1123 K, according to Zhou and Gulari, 1991). The silver crystalline films tested here do not seem attractive as substrates for STM of atomic resolution either, both because they show no atomic corrugation, even in freshly prepared films, and because crystalline terraces are often seen to move upon scanning. The troubles may be attributable to the presence of an oxide layer on the silver surface, since silver is considerably more susceptible to oxidation than gold

(Seizo, *et al.*, 1989).

Gold is known to be inert to the majority of chemical compounds. Nevertheless, halogens, thiols and disulfides are known to bind gold surfaces chemically and to produce stable images of 2-dimensional lattices in the STM. Thus, iodine and bromine, at low coverage, form a hexagonal lattice with a lattice parameter, **a** = 0.5 nm, corresponding to ($\sqrt{3}$x$\sqrt{3}$) R30° adlayer structure on Au(111) (McCarley and Bard, 1991; Haiss *et al.*, 1992; Tao and Lindsay, 1992). At high coverage (3x3) and (5x$\sqrt{3}$) structures, with lattice parameters up to 1.9 nm, are observed. The ($\sqrt{3}$x$\sqrt{3}$) R30° structure is also representative of organic thiols and disulfides on Au(111) substrates (Widrig *et al.*, 1991; Kim *et al.*, 1992).

Apart from halogens, thiol, and disulfides, other compounds have been reported to bind to Au(111) surfaces, producing 2-dimensional crystals. Roberts *et al.* (1989) were the first to use STM to study formation of stable adlayers of unidentified compounds on an annealed gold surface exposed to air. Howells *et al.* (1992) observed formation of a crystalline lattice of methyl isobutyl ketone. Schott *et al.* (1992) reported formation of ordered patterns of ferrocyanyl compounds. Yeo *et al.* (1992) have found a superlattice structure of n-decanol on Au(111) with a lattice parameter of about 1.7 nm. Tao *et al.* (1993) observed crystalline aggregates of DNA bases on Au(111) under potential control in electrolyte solution. Thus, gold is capable of binding substances other than halogens, thiols and disulfides.

Vapor deposition

Our tests of volatile compounds for their ability to bind Au(111), and to produce 2-dimensional lattices, considerably increases the number of such compounds as well as the number and possible types of 2-dimensional lattices into which they can be organized. Thus, the availability of a hydroxyl group in addition to the sulfhydryl group in mercaptoethanol molecules results in the formation of a 2-dimensional lattice, different from ($\sqrt{3}$x$\sqrt{3}$) R30°, which is characteristic of ethanethiol (Widrig *et al.*, 1991). This may be the result of strong interactions of OH-groups, making hydrogen bonds within the adlayer (as in the case of ethanol on HOPG studied by Morishige, 1992). There is little doubt that the SH-groups of mercaptoethanol are involved in binding to the Au surface, since we found mercaptoethanol to bind more strongly than other substances tested in agreement with a large number of experimental observations for organothiols (Nuzzo and Allara, 1983; Nuzzo *et al.*, 1987a, b; Porter *et al.*, 1987; Bain *et al.*, 1989; Enriquez *et al.*, 1992). It is capable of replacing other impurities on the surface. However, mercaptoethanol binding is reversible, with a characteristic desorption time (a few hours in pure argon) similar to that of alkanethiols in hydrocarbon solvents (20-200 minutes for different thioalkanes) (Bain *et al.*, 1989).

It is pointless to attempt modelling possible molecular arrangements of 2-dimensional lattices of mercaptoethanol, until more detailed studies are performed that measure the dependence of the unit cell image upon scanning characteristics, substrate and tip structure. Different images of the mercaptoethanol adlayer obtained under identical scanning conditions (Figs. 4A and 4B) can hardly be explained by differences in the packing of molecules, since the unit lattice structure is precisely the same in both images. We believe that difference in tip structure might be responsible for the observed differences in the distribution of state density in these cases. The same is true for 2-aminoethanol, which we find forms two types of lattices. Only the smaller one, with the lattice parameter of 0.48 $\pm$ 0.05 nm and 6-fold symmetry may be attributed to the ($\sqrt{3}$x$\sqrt{3}$) R30° structure. The second lattice cannot be described unambiguously in molecular terms, since the unit cell must contain several, possibly independent molecules, to account for its large lattice parameters (**a** = 1.7 nm, **b** = 1.5 nm).

The observed structures of 2-aminoethanol, acetic acid, water and ethanol as a result of their chemisorptive interaction with gold are not readily explained by known chemical precedents. We suggest that physical interactions, that remain to be characterized, underlie the ability of these and other compounds mentioned above to be adsorbed into well-organized 2-dimensional lattices. The physico-chemical basis of this non-specific binding requires further study. One suggestion that may account for the diversity of compounds binding gold is the possible involvement of hydrogen bonding with the oxygen atoms on the oxidized gold surface. Oxidation of the gold surface may occur during its annealing or cooling in a relatively low vacuum after evaporation, prolonged storage, or heat treatment in oxygen. In this regard, our attempt to anneal the surface at 500°C for 1 hour in a HV chamber at 10^{-6}-10^{-7} Torr resulted in a heavily contaminated surface with no visible atomic corrugation. Oxidation may explain the lack of an atomic gold corrugation visible in the majority of our controls and in those of Widrig *et al.* (1991), where only one of 30 samples studied displayed the atomic corrugation. Though the gold surface and the (111) plane, in particular (Chesters and Somorjai, 1975), is resistant to oxidation, oxide formation has been reported to proceed rapidly on (111)Au above 500°C at 10^{-6} Torr of oxygen or water (Chesters and Somorjai, 1975). Once formed, the oxide layer cannot be removed from the surface by heating in UHV for many hours (Chesters and Somorjai, 1975; Schrader, 1977). Low energy electron diffraction (LEED) experiments demonstrated that the oxide layer has a square mesh structure, with a lattice parameter **a** = 0.34 nm, incommensurate with the hexagonal reconstructed Au(111) lattice. Despite the fact that the oxide layer has never been seen in the STM as a regular structure (presumably due to its high flexibility under the action of thermal fluctuations and/or tip action), we cannot exclude its influence upon adlayer structure. In particular, worm-like structures, visible in the initial stage of the acetic acid adsorption (Fig. 5A) might represent a decoration of the structure of the underlying oxide. Their

smaller repeat, 0.37 ± 0.04 nm, seems to commensurate oxide lattice period. Very similar worm-like structures of adenine and guanine polymeric aggregates have been seen with repeat distances of 0.33-0.34 nm and a spacing of 0.7 ± 0.05 nm (Tao *et al.*, 1993).

Many of the compounds studied here are known for their ability to establish intermolecular hydrogen bonded links, which determine their structure in 3-dimensional crystals. We may expect that lateral hydrogen bonds within the adlayers also play a crucial role in the formation of 2-dimensional lattices. Thus, the acetic acid crystal consists of hydrogen-bonded chains where molecules are spaced by 0.43 nm (Johns and Templeton, 1958). Formation of such chains may present an alternative explanation for worm-like structures in adlayer of acetic acid observed in our experiments. Alcohols are also capable of forming chains (Pimentel and McClellan, 1960). However, the single hydroxyl of ethanol involved in chain formation provides no capability for hydrogen-binding with both the substrate and with other chains. This observation may account for the considerably lower m.p and b.p of ethanol (-130°C and 78°C), when compared to acetic acid (16°C and 117°C, respectively), as well as explaining less stable images of the ethanol adlayer as compared to those of acetic acid. In the case of ethanol, it is difficult to know whether we are dealing with a true 2-dimensional crystallization or with some physical phenomenon involving a dynamic instability in thin liquid films subjected to orientational forces as the tip moves.

The water adlayer is more stable than that of ethanol (in correspondence with higher m.p and b.p of water, reflecting more hydroxyls available for binding with the surface), but less stable, than that of acetic acid. The smallest lattice clearly seen at the top of Figure 7B, undoubtedly presents a 2-dimensional crystal with a lattice parameter, **a** = 0.8 ± 0.1 nm. This might be considered as a cubic structure of I_c ice, stabilized and distorted by interface forces: normally it has the lattice parameter, **a** = 0.635 nm, and is observed below 130 K (Mak and Zhou, 1992).

A good correlation in a series of b.p of volatile compounds (2-aminoethanol > acetic acid > water > ethanol) and stability of their STM images provides an argument in favor of hydrogen bonding as the main component of interactions between adsorbate and substrate. If so, we may expect a binding energy of about 40 kJ/mol for any group capable of forming hydrogen bonds to the surface oxygen. As shown in Appendix II, the binding energy needed to prevent molecules from displacements larger than their size during scanning can be estimated roughly to be 200-300 kJ/mol. These figures explain why small molecules may be observable only as crystalline species, where the lateral motion of individual molecules is strongly inhibited by the lattice and a low tip-support gap. Molecules, whose strong tendency for lateral interactions generates 2-dimensional crystals, liquid crystals, and lamellar structures, may be visualized with the STM, even on the relatively low-binding HOPG surface (Rabe and Buchholz, 1991; Buchholz and Rabe, 1992).

In terms of hydrogen bonding, the adsorbate monolayer may present enough target groups for formation of a second adsorbate layer and so on. Of course, the influence of the substrate will be diminished progressively as the distance from the layer to the surface increases, until the macroscopic forces of wettable films come into play, resulting in formation of micromicelles and bulk phase. It is not excluded that with the chemical potential of polar liquids dropping in the electrostatic field between tip and substrate as $(1/2)(\varepsilon_1-\varepsilon_g)\varepsilon_o E^2$ (E is field intensity, ε_1, ε_g and ε_o, are dielectric constants of liquid phase, vapor and vacuum, respectively), we have a liquid bridge between tip and surface, as has been demonstrated by Woodward *et al.* (1991) for water. This may explain observation of lamellar structures of volatile adsorbates at high bias voltages.

Sublimation

Of 4 condensed aromatic hydrocarbons deposited on HOPG, only coronene, with a symmetric arrangement of benzene rings was repeatedly imaged as a hexagonal 2-dimensional lattice, showing the same parameter, **a** = 1.1 nm; this corresponds to the p($\sqrt{21}$x$\sqrt{21}$) R10.9° superlattice, commensurate with graphite (0001) plane. Quite recently, this superlattice (lattice parameter **a** = 1.13 nm) has been observed with LEED by Zimmerman and Karl (1992). The inability of other flat aromatic hydrocarbons to produce regular structures may reveal difficulties in the 2-dimensional crystallization of irregularly shaped molecules on the symmetric HOPG surface, or incommensurability of their 2-dimensional lattices and that of basal graphite.

It is important to be aware that in sublimation deposition, we had no control on monolayer formation, and 3-dimensional crystals were often visible. Thus, we cannot exclude the possibility that pushing off the excess material by the tip, or dipping the tip into the layer of the sublimate, is a necessary condition for obtaining the 2-dimensional crystalline images observed. This has been well demonstrated recently by Allen *et al.* (1992) in parallel studies of adenine and thymine adlayer structures by STM and AFM methods.

According to estimates made in Appendix II, a barrier corresponding to 5-8 hydrogen bonds is necessary to hold a single molecule immobile when scanning. It is clearly valuable for the bond-making groups to be located on the molecule so as to be commensurate with binding centers of the substrate. The importance of this commensurability for high-resolution imaging of molecules has been stressed by Lippel *et al.* (1989), in attempting to explain their successful high-resolution imaging of separate copper-phthalocyanine molecules on a Cu(100) substrate. It is possible that the square symmetry of Cu-phthalocyanine molecules combines with the square symmetry of the oxide underlayer to enable our observation of these molecules with subnanometer resolution (Fig. 10). Rabe and Buchholz (1991) have also

noted the importance of the commensurability in imaging 2-dimensional molecular patterns on HOPG.

Electrospray deposition

According to calculations summarized in Appendix II, 20-60 hydrogen bonds are necessary to hold a flexible polymer molecules on the substrate, enabling them to be imaged as separate species. These interactions can prevent the whole molecules from displacements but do not necessarily stop intramolecular motion. Such motions, directed to saturate all possible intramolecular hydrogen bonds and other interactions, may explain why PVA and PEG molecules were observed as globular species (see Figures 14A and 14B, respectively) and not as polymer chains. Both PVA globules and PEG beads are oriented, presumably due to the action of tip motion.

Native protein molecules are not as flexible as PVA and PEG, so the number of hydrogen bonds needed to hold them can be reduced, relative to these polymers. We may expect, that in the few square nm contact area between a single protein molecule and the substrate, hydrogen bonds may be numerous. Specific for each protein-surface contact, the number and arrangement of the hydrogen bonding groups and their commensurability with substrate sites will vary enormously. This variation may, in turn, result in the very large variations in the extent of anchoring of different proteins, which is seen in the STM as large differences in the critical bias voltages.

Except for metallothionein, we did not observe internal structure in any protein: Our attempts to increase resolution resulted in pushing the molecules off the field of view, indicating that tip forces can become larger than those holding the molecule in a local position on the surface. A puzzling feature of protein images is that they are much more sensitive to bias voltage than to tunneling current. In addition, they are sensitive to the sign of the potential, so that when there is a negative voltage at the tip, images are usually less stable. We cannot presently explain these observations; they are especially puzzling, because of the weak dependence of the tip-substrate force on bias voltage, which Dürig *et al.* (1988) have determined by direct force measurements.

Oligomeric proteins may lose their quaternary structure when deposited by electrospray; this was demonstrated for hemoglobin, which produced images of two different types, presumably attributed to monomers and dimers. Often they were observed in the same screen (Fig. 11A). The images of different monomeric proteins deposited by the ES method have homogeneous sizes and shapes surprisingly close to those determined in X-ray analysis (Stryer, 1988). The only severe difference was found for the thickness of protein molecules, which did not exceed 1.3 nm in the best cases. This feature of STM images of protein molecules, noted in recent STM studies of proteins (Edstrom *et al.*, 1990) still remains to be explained, as does the mechanism of tunneling through thick condensed polymer layers.

The sizes and shapes of the monomeric protein molecules observed in our images are close to known sizes and shapes. Hence, it appears that complete unfolding of protein molecules has not occurred when they have been electrosprayed. This may be due to milder conditions in our spray technology, compared with those used in mass spectrometry. We have avoided the use of organic solvents and hot dry gases, as well as the procedure of ionic dehydration, by letting the sample collide with gas molecules in a prevacuum chamber. We cannot, thus, exclude the possibility that complete dehydration of protein molecules does not occur upon spraying. Dehydration by itself does not appear to trigger protein unfolding, since dry proteins are more stable (Mozhaev *et al.*, 1991) and rigid (Morozov and Morozova, 1990), than normally hydrated proteins. We believe that the perturbation of protein structure by the tip [for example, those phenomena postulated by Lindsay *et al.* (1991) to explain tunneling through protein globules] is responsible for the failure of attempts to see internal structure in globular proteins by STM.

One of the problems with the application of the electrospray method to deposition of biomacromolecules is the pH change that results from electrochemical charging of microdroplets. A droplet with a diameter of 1 μm, positively charged to 3 kV, has an excess of hydrogen ions, corresponding to pH = 2.5 in an unbuffered water droplet. Low pH is known to promote dissociation of tetrameric Hb into $\alpha\beta$-dimers (Ackers *et al.*, 1992). The presence of monomer-sized species in Hb images may result from this pH-induced dissociation.

In comparison with other methods of deposition, electrospray has the following advantages: **(1)** It provides a random distribution of deposited molecules over the surface, as opposed to the liquid deposition method. **(2)** No aggregation of the molecules as result of spraying is observed. **(3)** The substrate is free from direct contact with solvent. **(4)** Deposition of molecules at low temperature or in ultra high vacuum is possible. **(5)** The method facilitates a precisely-controlled deposition process via electrical means: For example, species separated in MS can be deposited on a substrate placed behind the MS slit. This idea of trapping separated molecules to study them further has been proposed by Meng *et al.* (1988). Realization of this by use of a tandem MS + STM technique opens intriguing capabilities for both chemistry and molecular biology (e.g., for sequencing biopolymer molecules).

Can the resolution of STM images of individual molecules be improved? First, tip-forming technology and scanning can both be refined further, so as to diminish the interaction of the tip with the adsorbed molecule. There is, however, an intrinsic lower limit for tip-adsorbate interaction at a given resolution, since the tunneling phenomenon is intimately bound up with the generation of mechanical force (Chen, 1991). Second, STM at low temperature should considerably diminish the forced lateral diffusion of molecules. However, decreasing the temperature reduces the requirements for binding energy

only slightly, since direct interaction with the tip is not likely to be very sensitive to temperature (see Appendix II). Third, more actively and strongly binding surfaces could be used. However, there is again a basic limit: When chemisorptive interactions with the surface become energetically comparable with those of the covalent bonds of molecules, the molecules may lose their chemical identity, and break. We believe that a careful optimization of all these parameters might provide a window for obtaining reliable images of separate molecules at high resolution.

Acknowledgments

This research has been supported by grants CA-24101 and GM-40746 (to NRK) and GM-29554 (to NCS) from the NIH, grant N00014-89-J-3078 from the Office of Naval Research (to NCS), and by Facilities for Biomolecular Imaging at NYU supported by funds from the W.M. Keck Foundation. We are grateful to Dr. J. Canary and Mr. Chang-Lin Chuang for providing us with metallothionein. One of the authors (VNM) is grateful to Dr. S. Lindsay for sending reprints, and unpublished manuscripts and consultations concerning technology of gold film preparation.

Appendix I: Estimation of the Contamination Rate of Surfaces in Gases and in Liquids

In this appendix we will consider the simplest case of very active molecules, binding to the surface irreversibly, when they reach it. Suppose the molecules are present in the surrounding medium at a concentration of $\mathbf{C_0}$ and consider two cases: (a) without stirring and (b) with stirring or flow of media around the sample.

Contamination rate without stirring

Consider one-dimensional diffusion with the boundary and initial conditions: $\mathbf{C}(\infty,t) = \mathbf{C_0}$, and $\mathbf{C}(x,0) = \mathbf{C_0}$, where the first argument corresponds to the distance from the surface, and the second is time. For a concentration gradient on the sample surface, we have (Gefreys and Swirles, 1962):

$$\mathbf{grad\ C(0,t)} = \mathbf{C_0}\,(\pi \mathbf{D}t)^{-1/2} \qquad (1.1)$$

Here **D** is the diffusion coefficient of the impurity molecules.

The specific time needed to saturate all the binding centers, **N**, of a surface of unit area may be obtained by equating the integral of diffusive flow, $\mathbf{J = D\ grad\ C(0,t)}$, to **N**:

$$N = \int_0^{\tau_1} J\,dt = C_0\,(D/\pi)^{1/2} \int_0^{\tau_1} t^{-1/2}\,dt = 2C_0\,(D\tau_1/\pi)^{1/2} \qquad (1.2)$$

Then for contamination time τ_1 we have:

$$\tau_1 = (\pi/D)\,(N/2\,C_0)^2 \qquad (1.3)$$

For example, oxygen at concentration of 1 ppm ($C_0 = 2.7\times10^{19} m^{-3}$) in argon under normal conditions will contaminate a surface with $N = 10^{19}\ m^{-2}$ in $\tau_1 = 1.7$ hours ($D = 1.8\times10^{-5}\ m^2/s$ for oxygen).

Contamination in a flow

As compared to the previous case, diffusion now proceeds through an unstirred layer. The thickness of the unstirred layer, δ_g, may be roughly estimated from the equation (Tunitskii, 1970):

$$\delta_g \approx (\nu L/V)^{1/2}\,(D/\nu)^{1/3} \qquad (1.4)$$

Here ν is a kinematic viscosity of the medium, **V** is flow rate, and **L** is the characteristic size of the sample.

The gradient of impurity concentration may be now estimated as $\mathbf{C_0}/\delta_g$ and the diffusive flux to binding surface can be written as:

$$\mathbf{J = D\ grad\ C} \approx \mathbf{D\ C_0}/\delta_g \qquad (1.5)$$

We will consider further only steady state diffusion processes. The time needed to cover all the surface is then easy to obtain, by equating $\tau_2\mathbf{J}$ to **N**:

$$\tau_2 \approx (\mathbf{N/DC_0})\,\delta_g = (\mathbf{N/DC_0})\,(\nu L/V)^{1/2}\,(D/\nu)^{1/3} \qquad (1.6)$$

One ppm of oxygen in argon ($\nu = 1.3\times10^{-5}\ m^2/sec$) flowing with rate of $V = 0.01$ m/s around a sample of $L = 5\times10^{-3}$ m in size, and having $N = 1\times10^{19}\ m^{-2}$ oxygen binding sites will be contaminated in $\tau_2 = 1$ minute.

It should be noted, that eqs. (1.3) and (1.6) give lower limits for contamination times, because in reality not every molecule striking a clean surface is bound, and because the calculations above do not account for reduction of the surface available for binding in the presence of adsorbate.

It is interesting to compare τ_1 and τ_2 with the characteristic time for surface contamination in a vacuum. For strongly binding impurities, the number of collisions of molecules per unit area in a unit time interval gives a flux **J** ($cm^{-2}\ s^{-1}$) (Roth, 1976):

$$\mathbf{J} = 3.5\times10^{22}\ \mathbf{P}\,(\mathbf{MT})^{-1/2} \qquad (1.7)$$

Here **M** (g) is the molecular weight of the impurity, **P** (Torr) is its partial pressure and **T** is the absolute temperature. Then for the contamination time we have:

$$\tau_\nu \approx \mathbf{N/J} = 2.8\times10^{-23}\ \mathbf{N\ P^{-1}}\,(\mathbf{MT})^{1/2} \qquad (1.8)$$

It is easy to calculate for oxygen, as the main constituent of low pressure gas in a vacuum chamber, that $\tau_g = \tau_2 = 1$ minute is characteristic of a vacuum of 4×10^{-8} Torr, and $\tau_\nu = \tau_1 = 1.7$ hours of 4×10^{-10} Torr. Thus, an atmosphere of ultrapure inert gas may provide conditions equivalent to high and ultrahigh vacuum with respect to the rate of surface contamination. Of course, equations (1.3) and (1.6) may also be used to estimate the contamination of surfaces in liquids.

Appendix II: Forced Surface Diffusion of Adsorbate

The diffusion coefficient of an adsorbate, D_s, is connected with its average life time, τ, in any given local position, via a simple relation (Barrer, 1967):

$$D_s = (1/4)\ \lambda_0^2\ \tau^{-1} \qquad (2.1)$$

with λ_0 denoting the distance between nearest neighbor binding sites on the surface. We may estimate τ as the stability of a bond. Rupture of this bond may be the result of thermal fluctuations in the case of free diffusion or the result of the combined action of thermal fluctuations and the lateral component of force from the scanning tip, F_τ. To account for the latter case, we may apply thermo-fluctuation theory of bond rupture (Regel *et al.*, 1974), which gives the life time of a stressed bond:

$$\tau = \tau_0 \exp[(U_0-\lambda_m F_\tau)/kT] \qquad (2.2)$$

Here, U_0 is the energy of the local binding, λ_m ($\approx 0.5\ \lambda_0$) is the lateral distance between minimum of the potential well and the position of the barrier, τ_0 ($\approx 10^{-14}$ sec), is the vibration frequency, k and T have their usual meaning of Boltzmann's constant and the absolute temperature.

Combining these two equations we obtain for the surface diffusion coefficient:

$$D_s = (1/4)\ \lambda_0^2\ \tau_0^{-1} \exp[-(U_0-\lambda_m F_\tau)/kT] \qquad (2.3)$$

Using the well-known relation between the diffusion coefficient and the root mean square displacement in a time interval Δt, $<\Delta x^2> = 4\ D_s \Delta t$, we may estimate the energy of binding needed to keep an adsorbate molecule within some limits of displacements, $<\Delta x^2>^{1/2}$, during the time of scanning, Δt:

$$U_0 > \lambda_m F_\tau - kT\ln(\tau_0 <\Delta x^2>/\lambda_0^2 \Delta t) \qquad (2.4)$$

According to this formula, to keep the adsorbate molecule from displacement by more than its dimension $<\Delta x^2>^{1/2}$ (= 0.5 nm), for Δt (= 10 sec), at a surface with λ_0 = 0.3 nm we need to have a binding energy of about 160 kJ/mol in the absence of tip forces. Taking estimates for tip-substrate interactions from the literature (Dürig *et al.*, 1988), and suggesting that the lateral component of force has the same order of magnitude, $F_\tau = 10^{-10}$-10^{-9} N, we obtain U_0 > 170-250 kJ/mol. These numbers correspond to 4-6 hydrogen bonds broken simultaneously.

Recent theoretical analysis of the surface diffusion of polymer molecules has shown that the activation energy for the diffusion of n-alkane chains grows with an increase in the number of links, N, as $U_0 = C\ N^\nu$, with ν = 0.56 (Cohen and Zeiri, 1992). Thus, to reach the necessary barrier of 170-250 kJ/mol, we should have 20-70 hydrogen bonds on the polymer chain.

These rough estimates give a scale of energies necessary for different conditions. For example, according to (2.4), decreasing the temperature from room temperature to that of liquid nitrogen will result in decreasing the required energy to 60-140 kJ/mol, corresponding to a factor of two.

Note, that the tip-adsorbate interaction will depend upon the resolution desired. Increasing the strength of the interaction may arise through mechanical contact at the small tip support gap needed for high resolution imaging. In addition, there is also, in principle, a direct connection between the tunneling current and the mechanical force (Chen, 1991): The force increases in direct proportion to the current used.

References

Ackers GK, Doyle ML, Myers D, Daugherty MA (1992) Molecular code for cooperativity in hemoglobin. Science **255**, 54-63.

Alexandrov ML, Gall LN, Verenchikov AN, Krasnov NV, Shkurov VA (1991) A study of mechanisms of cation production in mass-spectrometry. Nauchnoe Priborostoenie **2**, 1-36.

Allen MJ, Ballooch M, Subbiah S, Tench RJ, Balhorn R, Siekhaus W (1992) Analysis of adenine and thymine adsorbed on graphite by scanning tunneling and atomic force microscopy . Ultramicroscopy, **42-44**, 1049-1053.

Bain CD, Troughton EB, Tao Y-T, Evall J, Whitesides GM, Nuzzo RG (1989) Formation of monolayer films by spontaneous assembly of organic thiols from solution onto gold. J. Am. Chem. Soc. **111**, 321-325.

Barrer RM (1967) Surface and volume flow in porous media. In: The Solid-Gas Interface, Vol. 2. Flood EA (es.), Marcel Dekker, NY, pp. 557-609.

Buchholz S, Rabe JP (1992) Molecular imaging of alkanol monolayers on graphite. Angew. Chem. Int. Ed. Engl. **31**, 189-191.

Buchholz S, Fuchs H, Rabe JP (1991) Surface structure of thin metallic films on mica as seen by scanning tunneling microscopy, scanning electron microscopy and low-energy electron diffraction. J. Vac. Sci. Technol. **B9**, 857-861.

Chait BT, Kent BH (1992) Weighing naked proteins: practical mass measurement of peptides and proteins. Science **257**, 1885-1894.

Chen J (1991) Attractive interatomic force as a tunneling phenomenon. J. Phys.: Condens. Matter **3**, 1227-1245.

Chesters MA, Somorjai, GA (1975) The chemisorption of oxygen, water and selected hydrocarbons on the (111) and stepped gold surfaces. Surface Sci. **52**, 21-28.

Chowdhury SK, Chait BT (1991) Method of electrospray ionization of highly conductive aqueous solutions. Anal. Chem. **63**, 1660-1664.

Cohen D, Zeiri Y (1992) A theoretical study of the surface diffusion of large molecules. 1. n-alkane-

type chains on W(100). J. Chem. Phys. **97**, 1531-1541.

DeRose JA, Thundat T, Nagahara LA, Lindsay SM (1991) Gold grown epitaxially on mica: conditions for large area flat faces. Surface Sci. **256**, 102-108.

Dürig U, Zuger O, Pohl DW (1988) Force sensing in scanning tunneling microscopy: observation of adhesion forces on clean metal surfaces. J. Microsc. **152**, 259-267.

Edstrom RD, Meinke MH, Yang X, Yang R, Elings V (1990) Direct visualization of phosphorylase - phosphorilase kinase complexes by scanning tunneling and atomic force microscopy. Biophys. J. **58**, 1437-1448.

Enriquez EP, Kimberley HG, Guarisco VF, Linton RV, Mar KD, Samulski ET (1992) Behavior of rigid macromolecules in self-assembly at an interface. J. Vac. Sci. Technol. **A10**, 2775-2782.

Fenn JB, Mann M, Meng CK, Wong SF, Whitehouse CM (1989) Electrospray ionization for mass spectrometry of large molecules. Science **246**, 64-71.

Fotino M (1992) Nanotips by reverse electrochemical etching. Appl. Phys. Lett. **60**, 2935-2937.

Ganem B, Li Y-T, Henion JD (1991) Detection of noncovalent receptor-ligand complexes by mass-spectrometry. J. Am. Chem. Soc. **113**, 6294-6296.

Gefreys H, Swirles B (1962) Methods of Mathematical Physics. Cambridge Univ. Press, U.K., p. 565.

Haiss W, Lackey D, Besocke KH, Sass JK (1991) Atomic resolution scanning tunneling microscopy images of Au(111) surfaces in air and polar organic solvents. J. Chem. Phys. **95**, 2193-2196.

Haiss W, Sass JK, Gao X, Weaver MJ (1992) Iodine adlayer on Au(111) as discerned by atomic resolution scanning tunneling microscopy: relation to iodine electrochemical adsorption. Surface Sci. **274**, L593-L598.

Hallmark VH, Chiang S, Brown JK, Woll C (1991) Real-space imaging of the molecular organization of naphthalene on Pt(111). Phys. Rev. Lett. **66**, 48-51.

Howells S, Chen T, Gallagher M, Sarid D, Lichtenberger DL, Wright LL, Ray CD, Huffman DR, Lamb D (1992) High resolution images of single C_{60} molecules on gold (111) using scanning tunneling microscopy. Surface Sci. **274**, 141-146.

Ikonomu MG, Blades AT, Kebarle P (1991) Electrospray - ion spray. A comparison of mechanisms and performance. Anal. Chem. **63**, 1989-1998.

Johns RE, Templeton DH (1958) The crystal structure of acetic acid. Acta Cryst. **11**, 484-487.

Kim Y-T, McCarley RL, Bard AJ (1992) Scanning tunneling microscopy studies of Au(111) derivatized with organothiols. J. Phys. Chem. **96**, 7416-7420.

Kimura M, Otaki N, Imano M (1979) Rabbit liver metallothionein. Tentative amino acid sequence of metallothionein B. In: Metallothionein. Kagi JAR, Nordberg M (eds.). Birkhauser Verlag, Basel. pp. 163-168.

Krasnov NV, Muradimov MZ, Shevchenko SI (1991) Complex study of electrodynamic spraying parameters of liquids. Nauchnoe Priborostoenie **1**, 42-52.

Lindsay SM, Sankey OF, Schmidt KE (1991) How does the scanning tunneling microscope image biopolymers? Comments Mol. Cell. Biophys. **7**, 109-129.

Lindsay SM, Tao NJ, DeRose JA, Oden PI, Lyubchenko YL, Harrington RE, Shlyakhtenko L (1992) Potentiostatic deposition of molecules for scanning-tunneling microscopy. Biophys. J. **61**, 1570-1584.

Lippel PH, Wilson RJ, Miller MD Woll C, Chiang S (1989) High-resolution imaging of copper-phthalocyanine by scanning tunneling microscopy. Phys. Rev. Lett. **62**, 171-174.

Mak TCW, Zhou G-D (1992) Crystallography in Modern Chemistry: A Resource Book of Crystal Structures. Wiley Intersci. Publ. p. 107.

McCarley RL, Bard AJ (1991) Scanning tunneling microscopy studies of iodine adsorption on Au(111): direct observation of adlattice orientation. J. Phys. Chem. **95**, 9618-9620.

McLuckey SA, Van Berkel GJ, Glish GL, Huang EC, Henion, JD (1991) Ion spray liquid chromatography/ion trap mass spectrometry determination of biomolecules. Anal. Chem. **63**, 375-383.

Meng CK, Mann M, Fenn JB (1988) Of protons or proteins. Z. Phys. D. Atoms, Molecules and Clusters, **10**, 361-368.

Morishige K (1992) Structure and melting of a monolayer ethanol film on graphite. J. Chem. Phys. **97**, 2084-2089.

Morozov VN, Morozova TY (1990) What does a protein molecule look like? Comments Mol. Cell. Biophys. **6**, 249-270.

Mozhaev VV, Poltevsky KG, Slepnev VI, Badun GA, Levashov AV (1991) Homogeneous solutions of hydrophilic enzymes in nonpolar organic solvents. New systems for fundamental studies and biocatalytic transformations. FEBS Letters **292**, 159-161.

Nawaz Z, Cataldi TRI, Knoll J, Someck R, Petica JB (1992) STM imaging of molecules: factors affecting their reliability. Surface Sci. **265**, 139-155.

Nuzzo R G, Allara DL (1983) Adsorption of bifunctional organic disulfides on gold surfaces. J. Am. Chem. Soc. **105**, 4481-4483.

Nuzzo RG, Fusco FA, Allara DL (1987a) Spontaneously organized molecular assemblies. 3. Preparation and properties of solution adsorbed monolayers of organic disulfides on gold surfaces. J. Am. Chem. Soc. **109**, 2358-2368.

Nuzzo RG, Zegarski BR, Dubois LH (1987b) Fundamental studies of the chemisorption of organosulphur compounds on Au(111). Implications for molecular self-assembly on gold surfaces. J. Am. Chem. Soc. **109**, 733-740.

Ohtani H, Wilson RJ, Chiang S, Mate CM (1988) Scanning tunneling microscopy observation of benzene molecules on Rh(111)-(3x3)(C_6H_6 + 2CO) surface. Phys. Rev. Lett. **60**, 2398-2401.

Pimentel GC, McClellan AL (1960) The Hydrogen Bond. W. H. Freeman and Co., London. pp. 269-271.

Porter MD, Bright TB, Allara DL, Chidsey CED (1987) Spontaneously organized molecular assemblies. 4. Structural characterization of n-alkyl thiol monolayers on gold by optical ellipsometry, infrared spectroscopy and electrochemistry. J. Am. Chem. Soc. **109**, 3559-3568.

Rabe JP, Buchholz S (1991) Commensurability and mobility in 2-dimensional molecular patterns on graphite. Science **253**, 424-427.

Regel VR, Slutsker AI, Tomashevskii EE (1974) The Kinetic Nature of the Tensile Strength of Solids. Nauka, Moscow. pp. 108-138.

Reichelt K, Lutz HO (1971) Hetero-epitaxial growth of vacuum evaporated silver and gold. J. Cryst. Growth **10**, 103-107.

Robbins AH, Stout CD (1991) Crystal structure of metallothionein. In: Metallothionein. Stillman NJ, Shaw CF, Suzuki KT (eds.). VCH Publishers, New York. pp. 31-54.

Roberts CJ, Hoffmann-Millack B, Steer WS (1989) The observation of adsorbates on a gold surface in air: their deposition and removal using scanning tunneling microscopy. Surface Sci. **224**, 1-12.

Roberts CJ, Hoffmann-Millack B, Steer WS (1991) Observation of gold surface using scanning tunneling microscopy in an inert atmosphere and effect of water adsorption. J. Vac. Sci. Technol. **B9**, 841-844.

Roth A (1976) Vacuum Technology. North Holland Publ. Comp., Amsterdam. pp. 173-176.

Schott JH, Arana CR, Abruna HD, Petach HH, Elliott CM, White HS (1992) Substrate induced ordering of molecular adsorbates on Au(111). J. Phys. Chem. **96**, 5222-5224.

Schrader M (1977) Auger electron spectroscopic studies of chemosorption of oxygen to (111)-oriented gold surfaces. J. Colloid and Interface Sci. **59**, 456-460.

Seizo M, Morita S, Ishizaka T, Sugawara Y, Mishima S, Imai S, Mikoshiba N (1989) Surface conductance of metal surfaces in air studied with force microscopy. Japan J. Appl. Phys. Pt 2 **28**, L1634-L1636.

Smith T (1980) The hydrophobic nature of a clean gold surface. J. Colloid and Interface Sci. **75**, 51-55.

Smith DP, Hörber H, Gerber Ch, Binnig G (1989) Smectic liquid crystal monolayer on graphite observed by scanning tunneling microscopy. Science **245**, 444-447.

Smith RD, Loo JA, Edmonds CG, Barinaga CJ, Udseth HR (1990) New development in biochemical mass spectrometry. Anal. Chem. **62**, 882-889.

Sperling LH (1992) Introduction to Physical Polymer Science. Wiley-Intersci. p. 149.

Stryer L (1988) Biochemistry. W.H. Freeman and Co., New York. pp. 145, 158 and 406.

Tao NJ, Lindsay SM (1992) In situ scanning tunneling microscopy study of iodine and bromine adsorption on Au(111) under potential control. J. Phys. Chem. **96**, 5213-5217.

Tao NJ, DeRose JA, Lindsay SM (1993) Self-assembly of molecular superstructures studied by in situ scanning tunneling microscopy: DNA bases on Au(111). J. Phys. Chem. **97**, 910-919.

Thundat T, Warmack RJ, Allison DP, Ferrell TL (1992) Electrostatic spraying of DNA molecules for investigation by STM. Ultramicroscopy **42-44**, 1083-1087.

Tunitskii NN (1970) Diffusion and Random Processes. Nauka, Novosibirsk. Russia. p. 58.

Widrig CA, Alves CA, Porter MD (1991) Scanning tunneling microscopy of ethanthiolate and n-octadecanethiolate monolayers spontaneously adsorbed at gold interface. J. Amer. Chem. Soc. **113**, 2805-2810.

Woodward JT, Zasadzinski JAN, Hansma PK (1991) Precision height measurements of freeze fracture replicas using scanning tunneling microscope. J. Vac. Sci. Technol. **B9**, 1231-1235.

Yeo YH, McGonigal GC, Yackoboski K, Guo CX, Thomson DJ (1992) Scanning tunneling microscopy of self-assembled n-decanol monolayer at the liquid-gold(111) interface. J. Phys. Chem. **96**, 6110-6111.

Zhou XC, Gulari E (1991) Scanning tunneling microscopy of the annealing of a thin platinum film on highly oriented pyrolytic graphite. Acta Crystallogr. **47A**, 17-21.

Zimmerman U, Karl N (1992) Epitaxial growth of coronene and hexa-benzocoronene on MoS_2(0001) and graphite(0001): a LEED study of molecular size effects. Surface Sci. **268**, 296-306.

Discussion with Reviewers

T.G. Thundat: In contrast to DNA electrospray, where we observed lots of DNA aggregates directly beneath the spraying capillary (Thundat *et al.*, 1992), the authors do not observe any aggregate formation. Is the absence of aggregation in any way related to surface properties of protein?

Authors: We cannot explain the aggregation of DNA you mention, but this is useful to know about. One possibility might certainly be a difference in surface properties of proteins and DNA. Incomplete decomposition of sprayed microdroplets on their way to the substrate may be another reason for aggregation.

T.G. Thundat: Your discussion about the oxide formation on gold surface upon storage is not consistent with reports in the literature. If gold surfaces form an oxide, how can AFM see atomic resolution images on similarly prepared gold surfaces stored in air for many weeks?

Authors: Oxide formation after heat treatment of gold is well documented (some references are presented in the **Discussion**). AFM observation of atomic structure of gold might be a result of the removal of oxides by the tip due to dragging forces larger than in the STM.

T.G. Thundat: Presence of water on the surface (humidity) form a liquid bridge between the tip and the surface. The size of liquid bridge varies with relative humidity. Therefore, images of water on gold may be

due to noise. We have seen similar structures as shown in Figure 7A and 7B on mica surface at high humidity using AFM. This will also explain: "All the structures are readily reversible, except those of 2-mercaptoethanol: They fade out in a few minutes under a flow of pure argon".

Authors: It is not excluded, that there is a liquid bridge between the tip and the surface, but, this does not exclude crystallinity of water layer adjusting gold surface. It is difficult to explain the images of water on gold as a result of noise, since they have an appearance of regular polymorphic crystals. Minimal spacing in water 2-dimensional lattice corresponds to slightly distorted cubic I_c ice.

T.G. Thundat: Is it possible to move protein by changing tunneling current?

Authors: Yes, it is. But, many fold increase in current is required. We did not observed any noticeable changes in contrast when changing bias (see, e.g., Fig. 13).

T.G. Thundat: Did the authors observe $22x\sqrt{3}$ reconstruction of gold in air? How does the large area scan of the gold surface look? Do they observe islands, steps, slip planes etc.? How does the islands on gold influence the lamellar structure as shown in Figure 4c?

Authors: We did not try to observe gold surfaces in air. $22x\sqrt{3}$ reconstruction was occasionally observed under small glycerol droplets placed in the area of contact between the tip and the surface in argon flow-cell. It has a typical appearance of white parallel (distances by 6 ± 1 nm) and branched lines of about 0.01 nm in height (image at 40 mV, 11.6 nA or 386 mV, 20.6 nA); no gold atomic structure was noticed in these experiments.

Large area scans of gold surface looked different in different preparations [in terms of average size of good quality (111) planes and fraction of area they occupied]. Some preparations were similar to those described by DeRose *et al.* (1991). Islands, steps and slip planes were often observed. We did not make any attempt to systematically study these surface features.

Figure 4C shows that some lamellae cross step defects (bottom of the picture), though the influence of these on images is not drastic.

T.G. Thundat: How can gold surface be contaminated when it is stored in an inert atmosphere. The surface can be contaminated with water and hydrocarbons, such as deodorant, when exposed to room air.

Authors: We do not know the impurities that may be present in argon which may not be specified by the suppliers, or which may desorb from the glass walls, and contaminate the gold surface. Changes in gold surfaces under argon were also reported by Smith (1980).

H.J.K. Hörber: The interpretation of the double spots in Figure 11C, as a structure of the molecules, I do not believe. The orientation is, at all spots, the same, and there is no reason for a correlation in direction between the molecules. Therefore, I think, it is just a double tip effect.

R. Balhorn: Did samples imaged with different tips always yield structures with two lobes? Why should one lobe always appear less pronounced than the other (such an image could easily be produced by a double tip); was this result always obtained? If these two lobes really represent the two halves of the molecule, why are they all oriented in the same direction in the image? I would expect them to be randomly oriented.

Authors: A "double tip" artifact as an interpretation of Figure 11C was the first idea to come to our minds. We have reproduced double spotted images of metallothionein after spraying two different samples of metC (with and without bound Zn ions). In both cases double spot images prevailed. Figure 11D shows that double lobed molecules are imaged in the same field as monolobal ones; this undoubtedly cannot be explained as a double-tip effect (since part of the molecule images are not double spots) and strongly argues against the double-tip artifact. Similar relative orientation of metallothionein molecules can be easily explained as the result of the tip motion. Such an orientation due to tip motion also accounts for the observed extension of PVA molecules and PEG chains (Fig. 14).

H.J.K. Hörber: In the text, there are speculations about what really is on gold surfaces. As I learnt in talking with Jacob Israelachvilli, the first layer on gold surfaces after evaporation is a carbon monolayer, which in air starts to undergo chemical changes.

Authors: It is difficult to understand why carbon covered freshly prepared gold surfaces are highly hydrophilic.

H.J.K. Hörber: It is speculated that resolution of molecular structures can be achieved. The point that they have to be fixed on a certain plane, I think, is obvious. What is seen if they are fixed, depends on the electronic structures of the molecule and the surface and their interaction. Meanwhile, there are a lot of theoretical calculations about this. And with liquid crystals the results can be nicely reproduced.

Authors: We have not found in the literature an analysis of the energies needed to fix separate molecules so as to enable their STM imaging. The situation with respect to liquid crystals mentioned (and with all 2-dimensional crystals, in general) is very different.

H.J.K. Hörber: It is mentioned that the height of the molecules never exceeded 1.3 nm. I think this can be due to the fact that the rest of the solution sprayed also onto the surface stays there and the molecules stick in that stuff; the same happens with all the other preparation methods out of a solution. So, there is no advantage of the method on this point, and it is not true that the surface is not in contact with the solution.

Authors: First, control experiments did not show any noticeable changes in image of gold surface after spray-

ing pure solvent. Second, there was no dependence of heights of protein images on their X-ray sizes as in the case of lateral dimensions. All this makes unreasonable the interesting idea about protein molecules protruding through the layer of some stuff sprayed from solution.

H.J.K. Hörber: The discussion about forces applied in the STM to the sample is quite old and still not decided, as the final test is the experiment with a combined STM/AFM. Such experiments are performed in Rüschlikon at the moment, and Heini Rohrer told me, that he would think that the force is not connected to the tunneling current.
Authors: We are grateful to you providing us with the latest thinking about this problem.

S.M. Lindsay: Are you imaging real monolayers? If the tip is plunging through a thick insulating layer in order to tunnel, many interactions may serve to distort the 'image' in the interfacial region. Our paper (Lindsay *et al.*, 1992) demonstrates the effect using potential control of the interface to repeatedly deposit and then strip an insulating layer on Au(111). The adsorbate is seen clearly in AFM images, but is invisible in STM images where the tip just pushes its way through to image what appears to be 'clean' gold. Another example is given by what appears to be a purine monolayer on HOPG when imaged by STM, but is, in fact, dense rather rough aggregates when imaged by AFM (Allen *et al.*, 1992).
Authors: We think that we are imaging true monolayers in the case of vapor deposition (at least, in the first minutes of exposure), since the process of surface filling with adsorbate is monitored. We are not sure of this in the case of sublimation; here the cleaning of the surface with tip is possible.

S.M. Lindsay: The morphology of the gold surfaces is of some concern. The authors mention that the $23x\sqrt{3}$ reconstruction was observed, but also point out that their surfaces were often (deliberately) oxidized. We have studied this problem at some length using electrochemical control of the interface (here I take issue with the authors' reservations about electrochemical methods at the end of the third paragraph of the **Introduction**; their statement while technically true misses the point that there is considerably more control over an interface in electrochemical conditions than when it is in contact with a gas, the most important of which is the ability to alter surface charge, hence chemistry, over a wide range). The main source of 'artifacts' relating to the Au(111) surface is the reconstruction. Sites along the stacking faults have been shown to be reactive in UHV and we have studied this problem at the liquid-solid interface and in air and other gases. If the reconstruction is relieved rapidly, gold islands form on the surface, 'decorating' the reconstruction [see: Tao NJ, Lindsay SM (1992) Kinetics of potential induced $23x\sqrt{3}$ to 1x1 transition of Au(111) studied by in-situ scanning tunneling microscopy. Surface Science Letters **274**, L546-L553]. Another possibility is reaction of organic adsorbates at certain sites along the reconstruction; surface states can be formed which give bright spots in the images, one example is adenine on Au(111) (Tao *et al.*, 1993). With unknown contamination, anything is possible, but the general result is features that mirror the underlying geometry of the $23x\sqrt{3}$ reconstruction [Potentiostatic deposition of molecules for scanning Probe Microscopy. In: STM and SFM in Biology. Amrein A, Marti O (eds.), Academic Press, 1993, in press]. I make these points because we have not seen features like those shown in Figure 7B [water vapor on Au(111)] when we examine gold under clean aqueous electrolytes. If the lateral periodicity is 6-7 nm, then these could be features associated with a complex between contamination and sites along the reconstruction stripes.
Authors: We did not notice decoration of the $23x\sqrt{3}$ reconstruction (this might be due to surface oxidation). Some propensity for protein molecules to be more stable when located at steps was noticeable. As for water structures, in our experiments, the humidity was well below 100%, since usually water saturated argon was highly diluted with dry argon. Low activity of water and the presence of oxides might be definitive in obtaining the water structures presented in Figure 7B and responsible for absence of such features under aqueous electrolyte.

S.M. Lindsay: Was the electrospray done from a pure protein/polymer solution. If yes, then I worry about denaturation of the protein at low salt. If no, then I worry about the validity of the control experiment with pure water. Incidentally, why do you think that your control with pure water gave an unchanged gold surface while the experiment with water vapor gave what you refer to as "water crystals"?
Authors: Mostly, protein solutions in water were then thoroughly dialyzed against double-distilled water before electrospraying. The proteins used here (Mb, Hb, and Cyt-c) do not denature in pure water. Water electrosprayed at positive potential, used here, may penetrate the cell only in the form of stable hydronium ions, H_3O^+. On discharging on the gold surface, these produce water and hydrogen, which easily desorb from the surface (short exposure to water vapor and to pure hydrogen was shown to be completely and rapidly reversible). That explains why we did not see any changes of gold surface after electrospraying of water in control experiments.

S.M. Lindsay: One might expect that cutting the mica after depositing the Au would stress it. A characteristic sign of this damage is slip planes which lie at 60° [examples are shown in DeRose *et al.* (1991), we were not aware at the time that these feature were caused by damage to the gold]. Did you see any signs of such damage?

Authors: Sometimes we saw slip planes, like those shown by DeRose *et al.* (1991). But we cannot attribute them to the cutting procedure. They were relatively rare.

S.M. Lindsay: We have found that annealing above 350°C can cause roughening in places on the gold surface. Did you have any problem with this? How uniform were the films? Over what fraction of the surface was the $23x\sqrt{3}$ seen?
Authors: Annealing of the gold surface in our vacuum chamber for 1 hour at 500°C resulted in a highly oxidized surface (black holes, no atomic resolution). Short exposures to high temperature in air or oxygen (a few minutes) did not produce any noticeable roughening of the gold surface (except for loss of atomic structure). We cannot say about fraction of the surface displaying $23x\sqrt{3}$ reconstruction, since usually we used a z-scale too large to observe the reconstruction.

S.M. Lindsay: With reference to the 'holes' in mercaptoethanol layers: These have been reported for similar monolayer by several groups who used STM. We have carried out an AFM study (unpublished) and find that we do not see the holes. H. Rohrer (personal communication) has carried out simultaneous STM and AFM on such layers, concluding that they are due to electronic inhomogeneities and are not real 'holes'.
Authors: We are thankful for these important comments. We have an impression, that holes are rather, mobile. Sometimes, in scanning with bad (old) tungsten-tips, it is seen that they move and change their shape. This might be a result of indention of the tip through the oxide/adsorbate layer (and this explains why they are not visible in AFM mode). We tried to obtain images of the atomic structure of oxide layer, but failed to get reproducible structures, presumably, due to its rearrangement as a result of tip action or thermal motion.

S.M. Lindsay: Your result with proteins is intriguing. The dependence on voltage (but not current) indicates that you may be imaging via electrochemical currents in a water overlayer [see Yuan JY, Shao Z, Gao C (1991) Phys. Rev. Lett. **67**, 863].
Authors: Water content in ultra pure argon does not exceed 1 ppm (corresponds to a humidity level of less than 0.004%, much less than over silica gel!). It is thermodynamically highly improbable to have a water overlayer under this condition.

H.J.K. Hörber: I do not like speculations about surface contamination presented in the text, if there are ways to measure it with well established surface science techniques.
Authors: To answer the question raised by the referee, surface elemental analysis is required. Unfortunately, no equipment to perform surface analysis of gold contaminations is available in our laboratory. Also, we feel these would be beside the point of this article since we are not presenting an in depth analysis of the gold surface. We are describing methods of depositing solutes onto surfaces, that reveal details about these species. Presumably, someone interested in the surface of gold *per se* would undertake measurements of this kind, and write a different article.

R. Balhorn: In the studies with ethanol and water, how do the authors explain such a large lattice spacing (3.9-5.5 nm) for such small molecules?
Authors: This question concerns the possible interpretation of 2-dimensional crystals of small molecule in terms of possible packing. We tried to do that, but number of packings possible to account for given lattice is too big to make the procedure reliable without a proper assignment of observed features in distribution of height (current) within the unit cell to some properties of atoms, groups, or orbitals. An additional difficulty concerns some variability of images, illustrated in Figures 4A and 4B, which presumably reflects differences in tip structure. All this makes the problem of proper arrangement of adsorbed molecules from only STM data very difficult. Further experimental and theoretical studies are necessary, but are beyond the scope of this paper.

R. Balhorn: If the images of the proteins, polyvinyl alcohol, and PEG (Figures 11, 13, and 14) are really images of single molecules or aggregates, then one should be able to obtain an image characteristic of the surface in between these "molecules". Was this observed?
Authors: Yes. Characteristic image of initial gold surface (for example, black holes on aged supports) are readily seen after protein ES deposition.

R.L. McCarley: Is the tip insulated against Faradaic currents? Condensed water or other solvents would cause electrochemical currents to flow at the elevated biases used.
Authors: The tip had no insulation. Besides, the bias was only 22.9 mV in the experiment with water vapor, which is not enough to generate electrochemical current. Activity of water seems to be important. Crystals appear at non-saturating water pressure, where no water condensation is possible (as noted under experimental conditions, the flow of water saturated argon was diluted with that of pure one). No such crystals have been observed on gold under water (S.L. Lindsay, personal communication).

R.L. McCarley: How were the coronene images affected by potential bias variations?
Authors: We have not studied that.

R.L. McCarley: How do we know that the authors' gold has a stable oxide on it? X-ray photoelectron spectroscopy (XPS) must be done to show this.
Authors: This is presented in the paper as a hypothesis. Unfortunately, XPS is not available in our laboratory to experimentally prove this.